Tower- and Drone-Based BVOC Observations in a Suburban Tokyo Forest: Methodological Insights and MEGAN Comparison

Yujiro Ichikawa*[1], Katsuhito Yoshida[2], Shinichi Yonemochi[1], Kentaro Takagi[3], Atsuyuki Sorimachi[2], Kazuhide Matsuda[4], Toshimasa Ohara[5]

[1]Center for Environmental Science in Saitama, 914 Kamitanadare, Kazo City, Saitama, 347-0115, Japan

[2]Toyo University, 2100 Kujirai, Kawagoe City, Saitama, 350-8585, Japan

[3]Hokkaido University, Aza Tōkanbetsu, Horonobe Town, Teshio District, Hokkaido, 098-2943, Japan

[4]Tokyo University of Agriculture and Technology, 1528 Horinouchi, Hachioji City, Tokyo, 192-0355, Japan

[5]Asia Center for Air Pollution Research, 1182 Sowa Nishi-ku, Niigata City, Niigata, 950-2144, Japan

Correspondence to: Yujiro Ichikawa (ichikawa.yujiro@pref.saitama.lg.jp)

Abstract. Biogenic volatile organic compounds (BVOCs) substantially influence regional photochemical air pollution, climate, and the carbon cycle. However, observational constraints on BVOC emissions from urban or suburban forests in Asian megacity regions under humid subtropical climates remain limited. In this study, we conducted multi-year intermittent, multi-height BVOC observations at a 30 m flux tower in a suburban Tokyo forest dominated by *Quercus serrata*. Spatial variability was examined by combining tower measurements with supplemental drone-based sampling. The measurements were compared with estimates from the Model of Emissions of Gases and Aerosols from Nature (MEGAN). Isoprene volume mixing ratios increased during the warm-season observations from May to October, accounting for over 90% of the measured BVOC composition during peak summer, while monoterpenes remained low with weak vertical gradients. Isoprene exhibited distinct vertical volume mixing ratio gradients peaking within the canopy, with the daily average emission fluxes ranging from −0.05 to 15.30 mg m^{-2} h^{-1}. Drone-based measurements indicated horizontal variability in isoprene volume mixing ratios of approximately 10–30% within 30 m of the tower. Flux estimates derived from tower and drone measurements differed by approximately 30%, suggesting that small-scale spatial heterogeneity and height differences can affect gradient-based flux estimates. MEGAN generally overestimated the observed fluxes, particularly during the warm-season observations. These results demonstrate the potential of combining tower-based vertical profiling with supplemental drone-based horizontal sampling to evaluate BVOC fluxes and their spatial representativeness. Although the intermittent sampling design limits comprehensive seasonal and interannual interpretations, this study provides methodological insights for future tower- and drone-based BVOC observations and emission model evaluation based on canopy-scale measurements.

Keywords: BVOC, Isoprene, Emission, Flux measurements, Drone, Tower, MEGAN

1. Introduction

Terrestrial vegetation emits large amounts of biogenic volatile organic compounds (BVOCs), including terpenoids, alkanes, alcohols, carbonyls, esters, ethers, and fatty acids (Penuelas and Llusià, 2004; Yang et al., 2020; Tani and Mochizuki, 2021). Among these compounds, terpenoids account for a large proportion of BVOC emissions. Terpenoids primarily include isoprene (C_5H_8), monoterpenes ($C_{10}H_{16}$), sesquiterpenes ($C_{15}H_{24}$), and others. The estimated global annual emission of BVOCs is 1,007 Tg yr^{-1}, of which isoprene accounts for 535 Tg yr^{-1} (approximately 50% of the total annual emission) and monoterpenes for 157 Tg yr^{-1} (15%) (Guenther et al., 2012).

Many terpenoids exhibit high reactivity with atmospheric reactive species such as hydroxyl radicals (Atkinson and Arey, 2003), with isoprene and monoterpenes having atmospheric lifetimes ranging from tens of minutes to several hours. They contribute to the formation of tropospheric ozone (O_3) and secondary organic aerosols (SOA), thereby affecting air quality, climate, and the carbon cycle (Tani and Kawawata, 2008; IPCC, 2021). Therefore, improving observational constraints on BVOC emissions from forest ecosystems is important for air quality simulations and emission model evaluation.

In urban and suburban areas, BVOCs emitted from surrounding forests can influence photochemical air pollution, especially where anthropogenic nitrogen oxides are abundant. Model studies have suggested that BVOC emissions from vegetation surrounding large cities can make non-negligible contributions to ozone formation in urban areas, including the Pearl River Delta (Situ et al., 2013), Berlin (Churkina et al., 2017), and Tokyo (Chatani et al., 2015). These studies indicate that forests located near or upwind of major cities can act as important sources of reactive BVOCs. However, observational information on BVOC emissions from urban and suburban forests remains limited, particularly in Asian megacity regions under humid subtropical climates.

Numerical simulation models are used to evaluate the impact of chemical emissions on air quality by simulating physicochemical processes such as emission, reactions, transport, and deposition. The Model of Emissions of Gases and Aerosols from Nature (MEGAN), which is widely used to estimate BVOC emission fluxes from terrestrial vegetation, uses standardized basal emission rates as an input parameter (Guenther et al., 2006, 2012). However, the basal emission rates are often derived from enclosure measurements of individual leaves or branches, and scaling these measurements to canopy-scale fluxes can introduce substantial uncertainty because BVOC emissions vary with canopy position, vegetation structure, light environment, temperature, and plant stress. Micrometeorological methods provide canopy-scale flux estimates without directly disturbing vegetation and are therefore useful for evaluating emission models (Guenther et al., 2006; Tani et al., 2024). However, these methods also have important limitations. Flux estimates can be affected by complex canopy structure, terrain, roughness sublayer processes, assumptions regarding turbulent exchange, and chemical loss or transformation within and above the canopy. Therefore, micrometeorological fluxes should be interpreted with consideration of their methodological uncertainty. Complementary approaches, including enclosure measurements, vertical profiling, and spatially distributed sampling, can help constrain these uncertainties.

Micrometeorological BVOC flux observations have been conducted in various forest ecosystems worldwide (Fuentes et al., 1999; Fuentes and Wang, 1999; Baker et al., 2005; Holzinger et al., 2006; Ieda et al., 2006; Räisänen et al., 2009; McKinney et al., 2011; Bouvier-Brown et al., 2012; Fares et al., 2013; Miyama et al., 2013; Situ et al., 2013; Mochizuki et al., 2014, 2015; Bai et al., 2016; Emmerson et al., 2016; Rantala et al., 2016; Seco et al., 2017; Wei et al., 2018; Mochizuki et al., 2020; Bai et al., 2025; Dumont et al., 2026). Nevertheless, observations in urban and suburban forests near Asian megacities remain scarce. In the suburban forest of the Pearl River Delta region, Situ et al. (2013) measured BVOC fluxes using the relaxed eddy accumulation method from a 37 m tower; however, the observations were conducted for only several days during October–December 2010. Additional case studies are therefore needed to evaluate BVOC fluxes and model performance in suburban forest environments under humid subtropical conditions.

Most tower-based flux observations are conducted at a single fixed location, and their spatial representativeness is often difficult to assess. This issue is particularly relevant in heterogeneous forests, where vegetation structure, canopy height, and local meteorology can vary over short horizontal distances. Drone-based sampling provides a promising supplementary approach for examining horizontal variability around fixed towers. Although drone observations cannot replace tower measurements because of limited flight duration and sampling time, they can provide useful information on small-scale spatial heterogeneity and help interpret uncertainties in gradient-based flux estimates.

In this study, we conducted intermittent multi-year, multi-height BVOC observations at a 30 m flux tower in a suburban Tokyo forest dominated by *Quercus serrata* from June 2023 to October 2025. Isoprene emission fluxes were estimated using the aerodynamic gradient method. Drone-based measurements were conducted on selected days as a supplementary approach to examine horizontal variability near the tower and to evaluate the spatial representativeness of the tower observations. The observed fluxes were also compared with MEGAN estimates to assess model-observation agreement and possible sources of discrepancy. The objectives of this study were to: (1) characterize BVOC volume mixing ratios and isoprene fluxes observed by multi-height tower measurements during the intermittent sampling campaign, (2) evaluate small-scale horizontal variability using supplementary drone-based measurements, and (3) examine the agreement and discrepancies between observed isoprene fluxes and MEGAN estimates. Through these analyses, this study provides methodological insights into tower- and drone-based BVOC observations in suburban forest environments.

2. Methods

2.1 Site description

This study was conducted at the Field Museum Tamakyuryo (FM Tama), a research forest facility of Tokyo University of Agriculture and Technology located in the western suburb of Tokyo (35°38′18″N, 139°22′41″E), as shown in Fig. S1. A 30 m high scaffold flux tower has been constructed on the forest floor at FM Tama (168 m above sea level). This site has been extensively used to conduct numerous atmospheric observational and micrometeorological studies (e.g., Matsuda et al., 2015; Xu et al., 2021). Details regarding the FM Tama are described in Matsuda et al. (2015); they are briefly outlined below. The site covers approximately 20 hectares. The area around the flux tower is dominated by the deciduous tree *Quercus*

serrata, and the needleleaf tree *Japanese cedar* is also sparsely scattered throughout the site, creating a mixed forest character. The trees reach heights of approximately 20 m, with the canopy layer distributed between 10–20 m above ground level. *Q. serrata* began to grow lush foliage around April and shed its foliage by around November to December. In contrast, *J. cedar* is an evergreen tree and generally does not shed its leaves. The *J. cedar* trees at FM Tama are estimated to be approximately 50 years old (Naemura et al., 2003), and the *Q. serrata* trees are also presumed to be roughly the same age.

The wind rose for the observation period described in Section 2.2 is shown in Fig. S2. Prevailing winds were predominantly southerly, followed by northerly winds and, easterly winds, with westerly winds being rare. Together with the surrounding land use, this wind pattern suggests that BVOCs measured at the flux tower were mainly influenced by emissions from FM Tama under the sampled conditions. However, possible contributions from nearby vegetation outside the research forest cannot be completely excluded. Naganuma Park, a forest park, lies west of the flux tower, but westerly winds were infrequent during the observation period.

2.2 Observation design and sampling period

BVOC sampling was conducted intermittently from June 2023 to October 2025. Measurements were typically performed for 1–3 d per month, except during periods when sampling could not be conducted because of equipment maintenance, power outages, or unsuitable weather conditions. Rainy days were excluded from the analysis. In total, BVOC samples were collected on 34 sampling days during the study period. The observation dates, sampling schedules, sampling durations, number of samples, and representative meteorological conditions are summarized in Table S1. All times are expressed in Japan Standard Time (JST, UTC+9).

Sampling was typically conducted using 30 min integrated sorbent tube samples, during two daytime sampling windows: 10:00–12:00 and 14:00–16:00. Under the standard sampling scheme, four consecutive 30 min samples were collected during each window at each sampling height, resulting in up to eight samples per height per day. During the supplemental drone-based observations described in Section 2.6, the tower sampling duration was shortened to 15 or 17 min to match the drone sampling intervals and to fit within the available drone flight time and operational constraints. When samples were missing within the 10:00–16:00 daytime sampling window, daily averages were calculated only from the available observations. Note that these daily averages do not represent full diurnal averages.

The sampling design was intended to obtain multi-height BVOC observations under selected daytime conditions over multiple years, rather than to provide continuous flux measurements. Therefore, the dataset should be interpreted as multi-year intermittent observations. Monthly, seasonal and interannual features discussed in this study represent tendencies observed under the sampled conditions and should not be regarded as a complete climatology of BVOC emissions at the site. The main objectives of the observational design were to accumulate data and insights into tower-based BVOC flux measurements in a suburban forest, to examine the spatial representativeness of fixed-point observations using supplemental drone-based sampling, and to compare the observed isoprene fluxes with MEGAN estimates.

2.3 Meteorological observations

A three-dimensional ultrasonic anemometer (YOUNG, 81000) installed at the 30 m tower top measured horizontal and vertical wind directions and speed, as well as virtual temperature, and data were averaged over 10–30 min intervals. Additionally, an integrated weather sensor (VAISALA, WXT520) was installed at the flux tower heights of 25 m, 20 m, 17 m, and 1 m from June 2023 to November 30, 2023, and at 30 m, 24 m, 20 m, 17 m, 10 m, and 2 m between February 22, 2024 and October 2025 to measure air temperature, relative humidity, and horizontal wind direction and speed (Climatec CVS-HMP110 thermo-hygrometers and Climatec CYG-91000 anemometers were also used for some periods). The 10 min averages were used to obtain vertical profiles of each parameter. In cases where meteorological data could not be acquired at the flux tower due to maintenance or other reasons, measurements from the nearest Hachioji air quality monitoring station, which is managed by the Tokyo Metropolitan Government, were used.

Solar radiation including photosynthetic photon flux density (PPFD) was measured at 10 min intervals using a pyranometer (PREDE, PCM-01N) at 30 m height on the flux tower. The leaf area index (LAI) around the tower was measured for 1–3 d per month using a plant canopy analyzer (LI-COR LAI-2200). LAI was measured at four-fixed locations around the tower, and the average value of these locations was used. Therefore, LAI represents local canopy conditions around the tower rather than those of the entire FM Tama.

2.4 BVOC sampling and measurement

Based on the previously reported BVOC measurement conditions (Ichikawa et al., 2023), isoprene and seven monoterpenes (α/β-pinene, camphene, myrcene, 3-carene, limonene, p-cymene) were selected as target substances for measurement. BVOC samples were collected using an in-house sampling device as shown in Fig. S3. Air samples entering through the atmospheric inlet passed through a dehumidification tube (FUJIFILM Wako Pure Chemical, magnesium perchlorate, elemental analysis grade, 6–14 mesh) and an ozone scrubber cartridge (FUJIFILM Wako Pure Chemical, Presep-C Ozone Scrubber, potassium iodide). The air was then divided into four flow paths using a PTFE manifold. Each flow path was connected to a sorbent tube, with a two-way solenoid valve connected downstream. The opening and closing of the valves were controlled by a four-channel timer, enabling sample collection at different time intervals. All tubing was made of PTFE and the flow rate was set to 100 mL min^{-1}.

The sampling devices were installed at heights of 30 and 23 m above ground level, above the main canopy layer, at 17 m within the canopy, and at 3 m near the forest floor, as shown in Fig. 1 (a). Sampling was generally conducted between 10:00–16:00 using 30 min integrated sorbent tube samples; typically, four samples were collected in the morning and four in the afternoon.

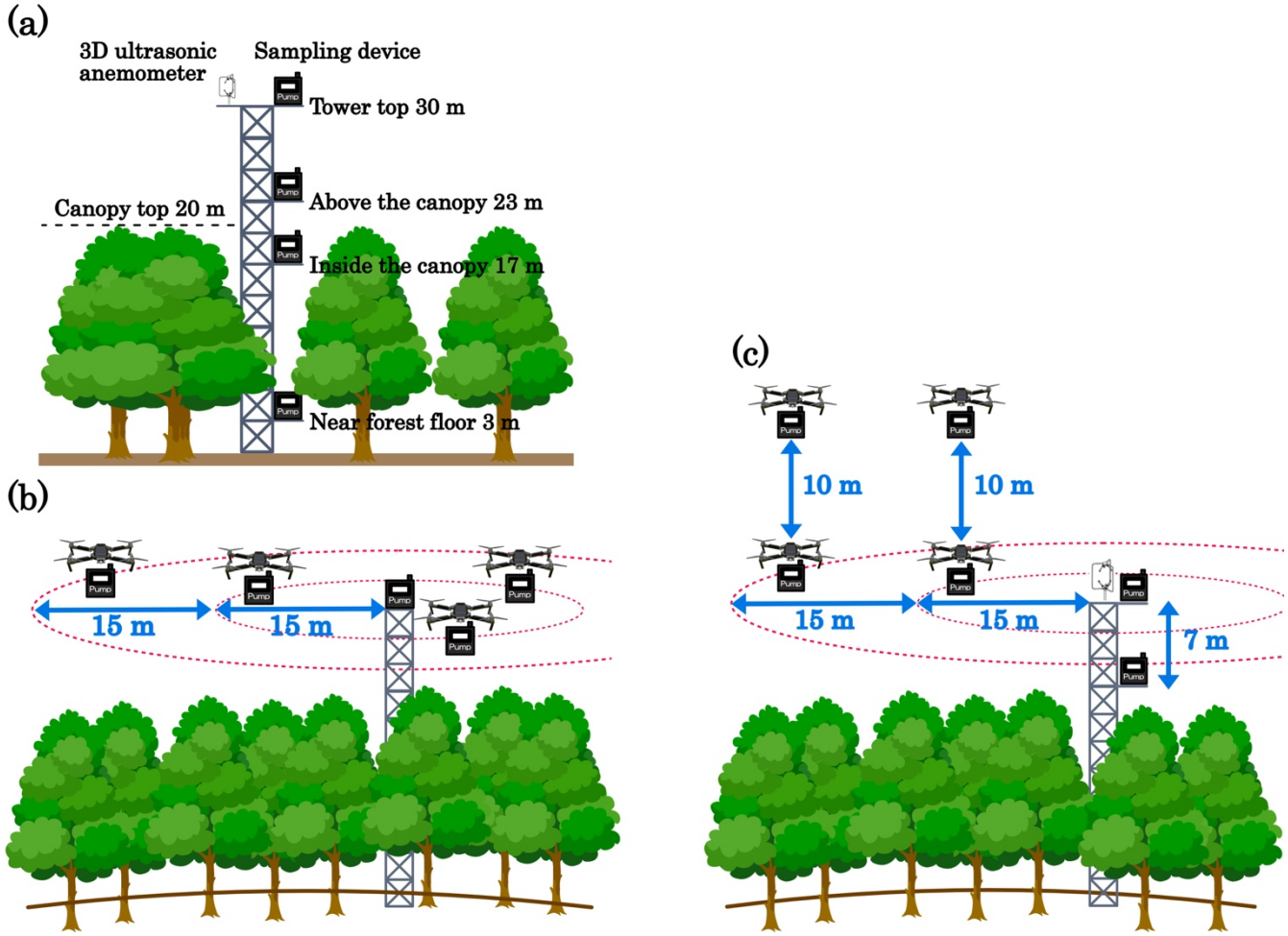

Figure 1: Schematic diagram showing the configuration of sampling equipment on the drone and flux tower, along with the observation points. (a) Observation method at multiple heights on the tower; (b) method for observing horizontal volume mixing ratio variations using the tower and drone; (c) method for observing horizontal flux variations using the tower and drone.

For the sorbent tube, Air Toxics (Camsco, multibed type packed with Carbograph and Carbosieve) was used from June 2023 to May 2024, and a manufacturer customized multibed type packed with Tenax TA and Carbotrap B (Camsco) was used from June 2024 to October 2025. Conditioning of the sorbent tubes was performed with a temperature program of 40°C (hold 1 min) →10°C min^{-1}→300°C (60 min) in a thermostatic chamber modified from a gas chromatography oven while high-purity nitrogen gas (>99.9999% purity) was flowing at a flow rate of 50 mL min^{-1}. Immediately after conditioning, the sorbent tubes were tightly closed at both ends with a brass cap using PTFE sealer, placed in stainless-steel containers with activated carbon, and stored in a glass desiccator under vacuum until sampling.

After sample collection, the sorbent tubes were tightly capped at both ends with brass caps, sealed in a desiccator with activated carbon to prevent contamination in an air-conditioned room, and stored until further analysis. Sample measurement was performed within 1 month of sampling.

Field blanks were used to evaluate potential contamination during transport, storage, field handling, and exposure associated with the sampling procedure. For each sampling campaign, blank sorbent tubes were transported to the field together with the sample tubes. During sampling preparation and after sample collection, the field blank tubes were uncapped and recapped at the same time as the sample tubes. During active sampling, the field blank tubes were kept capped and placed near the active sampling tubes. The field blanks were subsequently transported, stored, and analyzed in the same manner as the actual samples. The blank values were subtracted from the measured values of the corresponding samples. As the field blanks were not connected to the active sampling line, possible contamination or losses within the inlet and sampling line were not fully evaluated.

Preliminary recovery experiments were conducted to evaluate potential losses of the target BVOCs associated with the dehumidification tube and ozone scrubber cartridge. The recovery rates ranged from 64% to 129% among the target compounds: 87% for isoprene, 99% for α-pinene, 101% for camphene, 102% for myrcene, 64% for β-pinene, 79% for 3-carene, 71% for limonene, and 129% for p-cymene. The recovery exceeding 100% for p-cymene does not necessarily indicate contamination, but likely reflects experimental uncertainty associated with the recovery test, including analytical variability, uncertainty in standard preparation, and quantification uncertainty at low concentration levels. Although most compounds showed recoveries within approximately 70%–130%, β-pinene showed relatively lower recovery of 64%. These results indicate that large systematic losses were not observed for most target compounds, but compound-dependent uncertainty associated with the sampling pretreatment should be considered.

Based on the static dilution method described in the U.S. EPA published manual "TO-15A" (EPA, 2019), a fixed amount of each BVOC component standard solution dissolved in methanol (FUJIFILM Wako Pure Chemical, LCMS grade) was spiked into a clean inert stainless-steel vacuum canister (GL Sciences, GL-Scan). The canister was then heated at 60°C for 2 h to completely vaporize the components. After returning to room temperature, the canister was pressurized with VOC-free high-purity nitrogen gas (>99.9999% purity) to create a BVOC mixed standard gas. Toluene-d_8 (FUJIFILM Wako Pure Chemical, NMR grade, 99.5% purity) was used as the internal standard gas and was prepared in the same manner as described above.

BVOCs were analyzed using a gas chromatography–mass spectrometer (GC-MS; Shimadzu, GC-MS QP2010plus) connected to an automated thermal desorption system (PerkinElmer, TurboMatrix 650 ATD). Detailed measurement conditions are described in a previous study (Ichikawa et al., 2023). These devices undergo regular manufacturer inspections to ensure that they are in good condition and free of defects. The lower detection limit (3σ) was calculated from the standard deviation (σ) obtained from repeated measurements of the standard gas (n=5–7).

2.5 Flux calculation using the aerodynamic gradient method

According to Tani et al. (2024), *Q. serrata* emits isoprene but does not emit monoterpenes. As shown in the Section 3.1 below, volume mixing ratio of monoterpenes remained extremely low compared to isoprene, and sometimes fell below the detection limits. Considering that isoprene emission around the flux tower is primarily attributable to the dominant species *Q. serrata*, flux calculations were performed for isoprene only.

The aerodynamic gradient method (AGM) adopted in this study to determine isoprene emission flux is a micrometeorological method used to estimate fluxes of trace gases. The flux calculation in AGM is defined by Eq. (1) in accordance with Fick's first law (Erisman and Draaijers 1995; Fuentes, 1999; Räisänen, T. et al., 2009; Hayashi, 2010; Matsuda et al., 2010).

$$F_{\mathrm{obs}} = -K \cdot \frac{\partial C}{\partial z} = -\frac{u_* \cdot \kappa \cdot (C_{\mathrm{u}} - C_{\mathrm{l}})}{ln\left(\frac{z_{\mathrm{u}} - d}{z_{\mathrm{l}} - d}\right) - \Psi_{\mathrm{h}}\left(\frac{z_{\mathrm{u}} - d}{L}\right) + \Psi_{\mathrm{h}}\left(\frac{z_{\mathrm{l}} - d}{L}\right)} \quad (1)$$

where, F_{obs} is the observed flux (mg m^{-2} h^{-1}), K is the eddy diffusion coefficient (m^2 s^{-1}), C represents concentration (μg m^{-3}), z represents height (m), and the subscripts u and l denote two heights above the canopy (u > l). u_* is the friction velocity (m s^{-1}), κ is the empirically determined von Kármán constant (=0.41), Ψ_{h} is the integrated stability correction for heat, L is the Monin–Obukhov length, and d is the displacement height (m). u_* and L were derived from micrometeorological elements (e.g., horizontal and vertical wind speed, virtual temperature). The value of d was derived from the vertical wind profile measured at the FM Tama flux tower by Xu et al. (2021) (April–November: 16 m, December–March: 15 m).

Sampling was conducted primarily between 10:00 and 16:00 because the AGM is less suitable under stable nighttime or early morning conditions with weak turbulence (Erisman and Draaijers 1995; Tani et al., 2024). During the observation period, the average and median friction velocities for the entire period were 0.64 and 0.60 m s^{-1}, respectively, and no data points fell below 0.10 m s^{-1}, a threshold used by Räisänen et al. (2009) to exclude weak-turbulence conditions. These results indicate that turbulence was generally sufficient during the sampling period. However, it should be noted that flux estimates based on AGM are subject to uncertainties associated with the concentration gradient, the eddy diffusion coefficient, the stability correction, and the assumption that the selected measurement height lies within a layer of approximately constant flux.

2.6 Supplemental drone-based measurements

Supplemental drone-based measurements were conducted using a multi-rotor drone (DJI, Matrice 350 RTK) to evaluate the spatial representativeness of tower-based BVOC measurements under selected observational conditions. The drone was used as a supplementary platform for short-duration horizontal sampling around the tower, rather than as a replacement for continuous tower observations.

The swirling airflow generated by propeller rotation can cause atmospheric turbulence around the aircraft. If the placement of sample intake ports and measurement devices is not carefully considered, this turbulence may affect measurement accuracy and precision. However, it has been noted that many previous studies using drones do not address countermeasures

for this swirling airflow (Altamira-Colado et al., 2024). Based on computational results from a fluid model by McKinney et al. (2019) and preliminary tests using the actual aircraft, the sample inlet, dehumidification tube, ozone scrubber cartridge and sorbent tube were mounted on a titanium support extending approximately 60 cm above the drone body, as shown in Fig. 2. This configuration was designed to reduce the influence of propeller induced airflow and aircraft vibration on the sampled air.

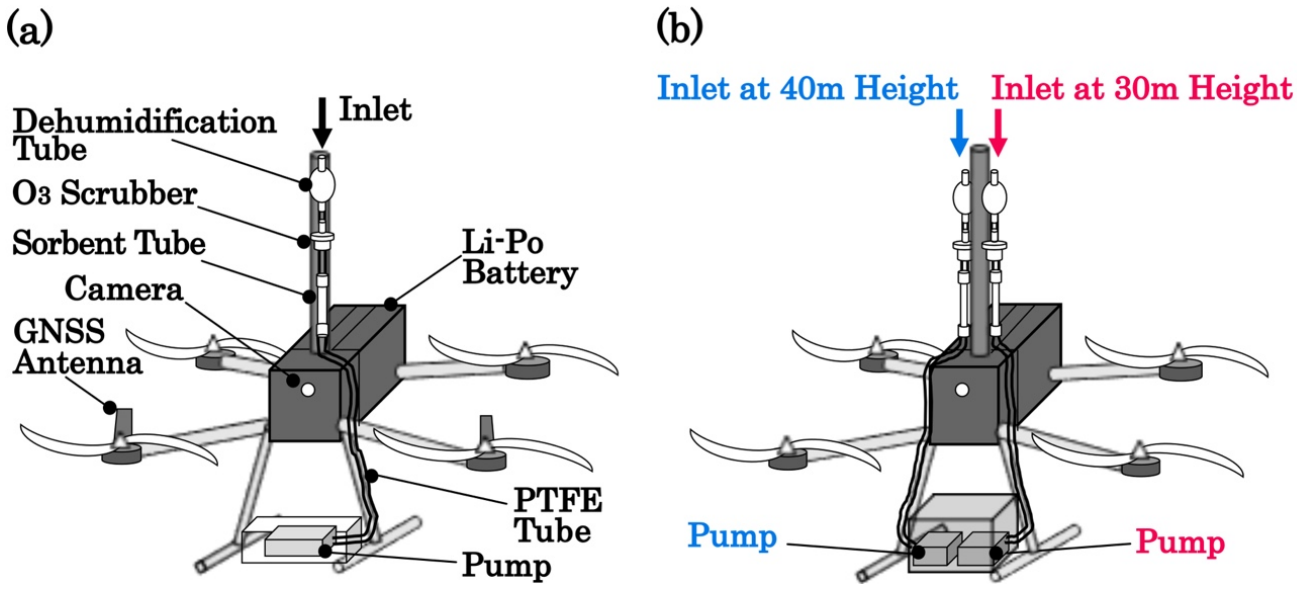

Figure 2: Status of equipment installed for BVOC sampling using a drone. (a) Installation for horizontal volume mixing ratio variations, and (b) installation for horizontal flux variations.

On October 12, 2023, July 23, 2024, and June 17, 2025, simultaneous tower and drone measurements were conducted at 30 m height. As shown in Fig.1 (b), the drone sampled air at four locations approximately 15–30 m from the tower at different azimuths to evaluate horizontal variability in BVOC volume mixing ratios. The flight position was determined by acquiring positional data via the Global Navigation Satellite System (GNSS) antenna and was visually monitored from the tower. After arriving at each observation point, the drone hovered briefly to stabilize before sampling was initiated using the pump timer function. The stability of the drone at its fixed position during hovering is shown in Fig. S4. The drone equipment mounting method for these observations is shown in Fig. 2 (a), and each sampling period lasted 15 min. The flight altitude was precisely measured relative to the tree canopy using its onboard altitude sensor.

On July 29, 2025, an additional drone experiment was conducted to examine the sensitivity of gradient-based flux estimates to sampling location and height intervals, as shown in Fig. 1(c). Drone samples were collected at 30 and 40 m, and fluxes were calculated using the AGM equation in the same manner as for the tower observations. The configuration of equipment installed for this observation is shown in Fig. 2 (b), which carried two pumps and other equipment. Due to safety

concerns, the drone did not collect samples at altitudes below 30 m, so the altitude differs from that of the tower. After completing the first sampling at a height of 30 m at the observation point, the aircraft ascended vertically to 40 m and performed another sampling. As the drone payload limit prevented the installation of a three-dimensional ultrasonic anemometer, micrometeorological parameters measured at the tower were used for the drone-based flux calculation. This calculation assumes that the tower and drone sampling heights were influenced by similar micrometeorological conditions and that the selected height interval was suitable for a gradient-based flux estimate. As the same tower-derived micrometeorological parameters were used for the tower- and drone-based AGM calculations, differences between the tower- and drone-derived flux estimates mainly reflect differences in the measured concentration gradients and sampling height intervals. However, possible horizontal differences in turbulence caused by local canopy roughness, terrain, or flow distortion could not be evaluated. Therefore, drone-derived fluxes should be interpreted as an exploratory assessment of spatial representativeness and methodological uncertainty under tower-derived turbulence conditions, rather than as an independent quantitative validation of the tower-based fluxes.

2.7 MEGAN calculation and model evaluation

We compared the tower-based observed isoprene emission fluxes with model calculations from MEGAN (Guenther et al., 2006, 2012), an extensively used BVOC emission estimation model, to evaluate model–observation agreement under the sampled conditions. MEGAN calculations were conducted at a 10 min time resolution for the daytime period from 10:00–16:00 for each day from June 1, 2023 to October 31, 2025. Thus, the model was run continuously for the daytime sampling window throughout the study period, rather than only for the individual observation days. For comparison with the observations, model outputs corresponding to the actual sorbent tube sampling times were extracted and paired with the observed fluxes. Additionally, PPFD, meteorological variables, and LAI data were obtained as described in Section 2.3. The comparison therefore represents model–observation agreement during the sampled daytime periods and should not be interpreted as an evaluation of full-day emission estimates. The estimation of isoprene emission flux F_{cal} (mg m^{-2} h^{-1}) was performed using the following Eq. (2), with parameters set based on the original literature for MEGAN (Guenther et al., 2006, 2012).

$$F_{\mathrm{cal}} = \varepsilon \cdot \gamma_P \cdot \gamma_T \cdot \gamma_{LAI} \cdot \gamma_{age} \cdot \gamma_{SM} \cdot \gamma_{\mathrm{CO_2}} \cdot \rho \quad (2)$$

where, ε is the basal emission rate under standard conditions for the plant functional type (PFT), and we adopted the standard value of 10 mg m^{-2} h^{-1} for isoprene from broadleaf deciduous temperate trees (Guenther et al., 2012). The standard conditions for MEGAN are described in Guenther et al. (2006, 2012); for example, a leaf temperature of 30°C, PPFD of 1500 μmol m^{-2} s^{-1}, and a standard canopy structure ($\mathrm{LAI_{std}}$) of 5. Although a PPFD of 1000 μmol m^{-2} s^{-1} is typically used as the standard condition at the leaf level in the G93 algorithm (Guenther et al., 1993), MEGAN uses 1500 μmol m^{-2} s^{-1} at the canopy scale. The γ terms represent activity factors related to environmental and phenological conditions, where γ_P for light response, γ_T for temperature response, γ_{LAI} for LAI, γ_{age} for leaf age, γ_{SM} for soil moisture response, and $\gamma_{\mathrm{CO_2}}$ for carbon dioxide response. The escape efficiency ρ, which is the proportion of isoprene emitted from the canopy that escapes into the

upper atmosphere, was set to 0.96 following Guenther et al. (2006). The settings of the activity factors used in this study are described below.

300

2.7.1 Activity factor for light response γ_P

The light dependent activity factor γ_P was calculated every 10 min using Eqs. (3) – (5).

$$\gamma_P = 0 \text{ for } \sin(a) < 0 \quad (3a)$$

$$\gamma_P = \sin(a)\left\{2.46 \cdot \left[1 + 0.005 \cdot \left(P_{daily} - 400\right)\right] \cdot \phi - 0.9 \cdot \phi^2\right\} \text{ for } \sin(a) > 0 \quad (3b)$$

305

$$\phi = \frac{P_{\mathrm{ac}}}{(\sin(a) \cdot P_{\mathrm{toa}})} \quad (4)$$

$$P_{\mathrm{toa}} = 3000 + 99 \cdot \cos\left(2 \cdot 3.14 \cdot \frac{(DOY - 10)}{365}\right) \quad (5)$$

where, a is solar angle (degrees), P_{daily} is daily average above canopy PPFD (μmol m^{-2} s^{-1}), φ is the above canopy PPFD transmission factor (non-dimensional), P_{ac} is the above canopy PPFD (μmol m^{-2} s^{-1}), P_{toa} is PPFD at the top of the atmosphere (μmol m^{-2} s^{-1}), and DOY is the day of year. The solar angle a was calculated from the latitude of FM Tama, the

310 solar declination, and the hour angle.

2.7.2 Activity factor for temperature response γ_T

The temperature dependent activity factor γ_T was calculated using Eqs. (6) – (9).

$$\gamma_T = \frac{E_{\mathrm{opt}} \cdot \mathrm{C_{T2}} \cdot \exp\left(\mathrm{C_{T1}} \cdot \chi\right)}{\{\mathrm{C_{T2}} - \mathrm{C_{T1}} \cdot [1 - \exp(\mathrm{C_{T2}} \cdot \chi)]\}} \quad (6)$$

315

$$\chi = \frac{\left[\left(\frac{1}{T_{\mathrm{opt}}}\right) - \left(\frac{1}{T_{\mathrm{hr}}}\right)\right]}{0.00831} \quad (7)$$

$$E_{\mathrm{opt}} = 1.75 \cdot \exp\left(0.08 \cdot \left(T_{\mathrm{daily}} - 297\right)\right) \quad (8)$$

$$T_{\mathrm{opt}} = 313 + 0.6 \cdot (T_{240} - 297) \quad (9)$$

where, T_{hr} is the hourly average air temperature (K), T_{daily} is the daily average air temperature (K), E_{opt} is the maximum normalized emission capacity, T_{opt} is the temperature at which E_{opt} occurs, T_{240} is the average air temperature over the past

320 240 h (K), and $\mathrm{C_{T1}}$ (=80 kJ mol^{-1}) and $\mathrm{C_{T2}}$ (=200 kJ mol^{-1}) are empirical coefficients that represent the energies of activation and deactivation, respectively (Guenther et al., 1999, 2006). For calculating 10 min values of γ_T, the hourly average air temperature corresponding to each model time step was used as T_{hr}. The temperature history term T_{240} was calculated from continuous meteorological data over the preceding 240 h, rather than from daytime data only. This allowed γ_T to account for antecedent thermal conditions before each daytime model time step.

325

2.7.3 Activity factor for LAI γ_{LAI}

The activity factor for LAI, γ_{LAI}, was estimated using Eq. (10).

$$\gamma_{LAI} = \frac{0.49 \cdot LAI}{\sqrt{1 + 0.2 \cdot LAI^2}} \quad (10)$$

As LAI was measured intermittently, the LAI value from the closest observation date was used for each model calculation day.

2.7.4 Activity factor for leaf age γ_{age}

The leaf age activity factor γ_{age} was estimated using Eq. (11).

$$\gamma_{age} = F_{new} \cdot A_{new} + F_{gro} \cdot A_{gro} + F_{mat} \cdot A_{mat} + F_{old} \cdot A_{old} \quad (11)$$

where F represents the proportion of leaves in each age class, A denotes the leaf age-specific activity factor, and the subscripts new, gro, mat, and old indicate new, growing, mature, and old leaves, respectively. The values for A for isoprene are summarized in the table presented by Guenther et al. (2012), with A_{new}=0.05, A_{gro}=0.6, A_{mat}=1.0, and A_{old}=0.9.

Based on field observations of *Q. serrata* at FM Tama, the leaves emergence generally occurred between April to May, mature leaves dominated from June to mid-September, leaf coloration and senescence occurred from mid-October to November, and leaves were mostly absent from December to March. Based on these local phenological observations, the monthly fractions of each leaf age class were set as shown in Table S2. As *Q. serrata* is deciduous and leaves were mostly absent from December to March, γ_{age} was set to 0 during this period.

2.7.5 Activity factors for soil moisture γ_{SM} and carbon dioxide γ_{CO2}

Soil moisture data (volumetric water content, $m^3\ m^{-3}$) were obtained from ERA5-Land (Muñoz-Sabater et al., 2021), a land surface dataset provided by the European Centre for Medium-Range Weather Forecasts. Soil moisture varies significantly with depth, and whether plants can absorb water depends on root depth (Guenther et al., 2006). We calculated weighted daily averages of soil moisture content at a spatial resolution of 0.1° for three soil layers (layer 1: 0–7 cm, layer 2: 7–28 cm, layer 3: 28–100 cm) around FM Tama. The calculated values ranged from 0.17–0.43 $m^3\ m^{-3}$. Based on these values, we assumed that severe soil moisture stress was unlikely during the calculation period and γ_{SM} was set to 1.

As the area surrounding FM Tama is residential, CO_2 concentrations during the observation period are expected to show no significant variation from those in the general atmospheric environment. Therefore, the influence of CO_2 on isoprene emissions was assumed to be constant. Therefore, γ_{CO_2} was set to 1 for the entire period.

2.7.6 Comparative evaluation of observed and MEGAN calculated values

The correspondence and error characteristics between F_{cal} and F_{obs} were evaluated. To calculate the degree of systematic overestimation or underestimation of the model, the mean bias error (MBE) was determined using Eq. (12).

$$\mathrm{MBE} = \frac{1}{N}\sum_{i=1}^{N}(F_{cal,i} - F_{obs,i}) \quad (12)$$

where N is the number of data points used for comparison. A positive MBE indicates model that the overestimates, whereas a negative MBE indicates model underestimation.

Furthermore, as a comprehensive indicator for evaluating the magnitude of model error, the root mean square error (RMSE) was calculated using Eq. (13).

$$\mathrm{RMSE} = \sqrt{\frac{1}{N}\sum_{i=1}^{N}(F_{cal,i} - F_{obs,i})^2} \quad (13)$$

The closer this statistical indicator approaches its minimum value of 0, the closer the calculated value is to the actual measured value.

As the observations were intermittent and limited to selected daytime periods, these statistics were used to evaluate model–observation differences under the sampled conditions rather than for assessing full seasonal model performance.

3. Results

3.1 BVOC composition during the intermittent sampling campaign

Figure 3 summarizes the monthly average volume mixing ratios of the eight target BVOC species at each sampling height during the intermittent sampling campaign. The corresponding numerical values are summarized in Table S3. The averages reported in this section were calculated from available daytime samples collected between 10:00 and 16:00 on the observation days and should therefore be interpreted as summaries of the sampled conditions rather than complete monthly averages.

From November to April, volume mixing ratios of all target compounds were generally low at all heights. In contrast, from May to October, isoprene volume mixing ratios increased markedly, with several samples exceeding 10,000 pptv during July and August. During peak summer observations, isoprene accounted for more than 90% of the measured BVOC composition at all heights (Fig. S5). Although the detailed mechanisms underlying isoprene emission in plants remain incompletely understood, the widely accepted explanation is that it protects leaves from high temperatures (Sharkey et al., 2008). This study also observed a tendency for isoprene volume mixing ratios to increase during periods of high temperature.

Monoterpene volume mixing ratios were much lower than those of isoprene throughout the campaign. Among the measured monoterpenes, α-pinene, limonene, and p-cymene were relatively abundant, but each generally accounted for only about 1–2% of the total measured BVOC volume mixing ratio during summer observations. Distinct vertical gradients of monoterpenes were not evident. These results are consistent with previous reports that *Q. serrata* is primarily an isoprene-emitting species and emits few monoterpenes (Tani et al., 2024). Therefore, the following sections focus on isoprene.

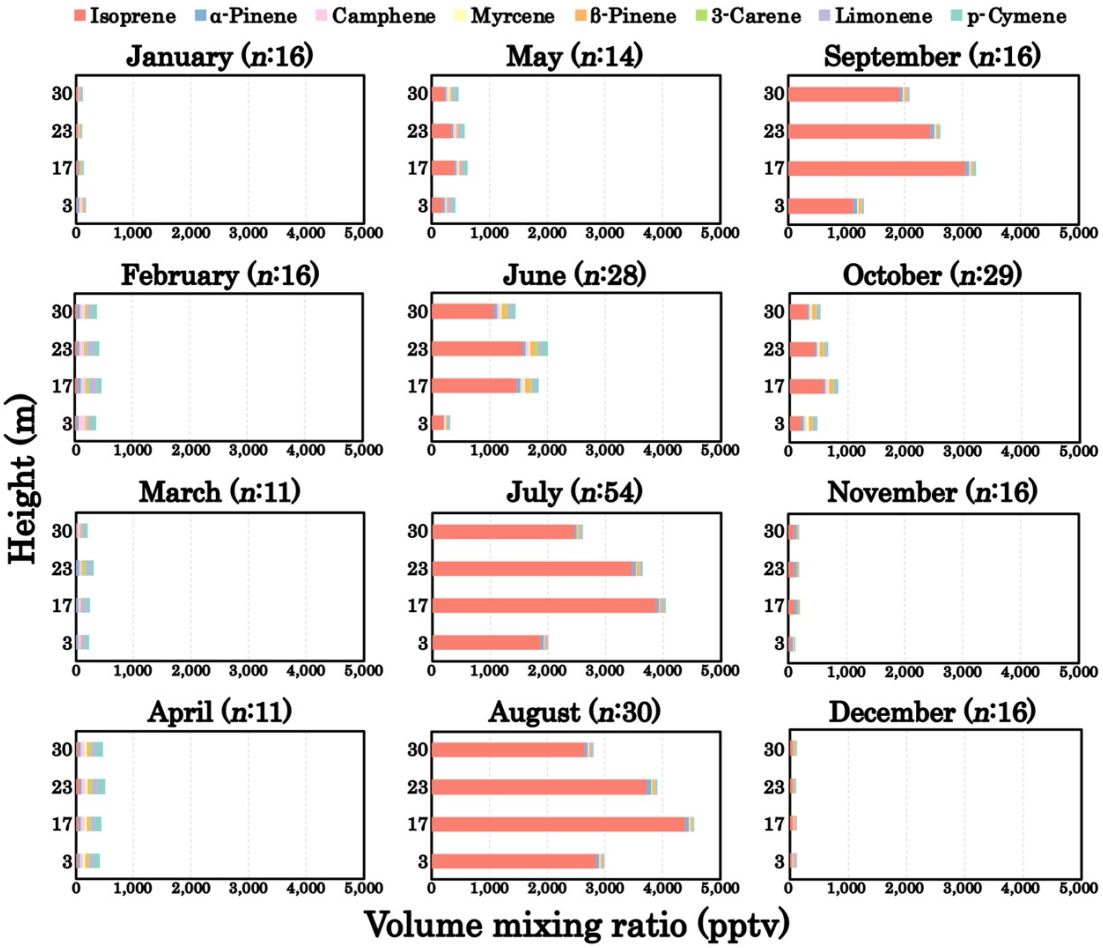

Figure 3: Monthly average volume mixing ratios (pptv) of the eight target BVOC species at each sampling height during the intermittent sampling campaign. Monthly averages were calculated from available daytime samples collected on the observation days.

3.2 Vertical profiles of isoprene

Figure 4 shows the vertical distribution of isoprene volume mixing ratios at different heights. The boxes represent the 25th–75th percentile ranges, the whiskers represent the 2nd–98th percentile ranges, and the median and average are overlaid.

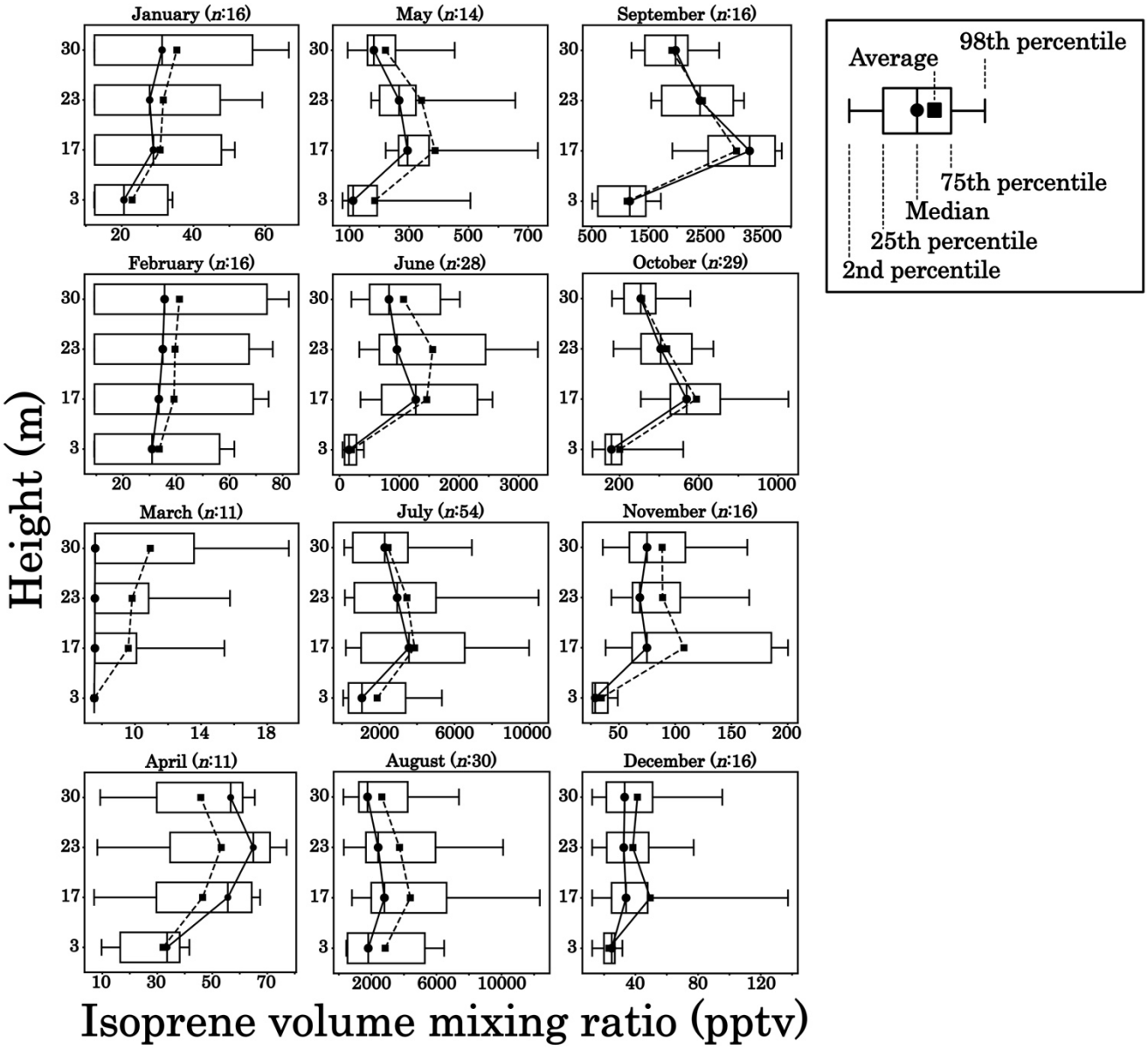

Figure 4: Boxplots overlaid with average values showing the monthly distribution of isoprene volume mixing ratios by height during the intermittent sampling campaign. The solid and dashed lines connect the median and average values for each height, respectively.

During the warm-season observations (May to October), when *Q. serrata* leaves were densely foliated, isoprene volume mixing ratios were generally highest at 17 m, corresponding to the canopy layer. The distributions at 17 m showed higher upper-percentile values than those at the other heights, indicating that enhanced isoprene volume mixing ratios were frequently observed within the canopy, where *Q. serrata* leaves were concentrated (the canopy range of 10–20 m). At 23 and

30 m, above the main canopy layer, the distributions also showed extended upper tails during the warm-season, suggesting upward transport of isoprene emitted from the canopy. In contrast, isoprene volume mixing ratios at 3 m near the forest floor were generally lower and showed narrower distributions.

During the cold-season observations (November to April), isoprene volume mixing ratios were low at all heights, and clear vertical gradients were not evident. These results indicate that the vertical structure of isoprene was most apparent during the foliated warm-season period.

3.3 Tower-based isoprene emission flux observations and environmental relationships

Figure 5 shows the daily average isoprene emission fluxes (F_{obs}) calculated from the vertical gradient of isoprene concentration between 23 and 30 m. Canopy temperature and PPFD during the observation days are also shown in Fig. 5. The daily average values and standard deviations for F_{obs} and related meteorological parameters are summarized in Table 1. F_{obs} ranged from −0.05 to 15.30 mg m^{-2} h^{-1} during the observation period.

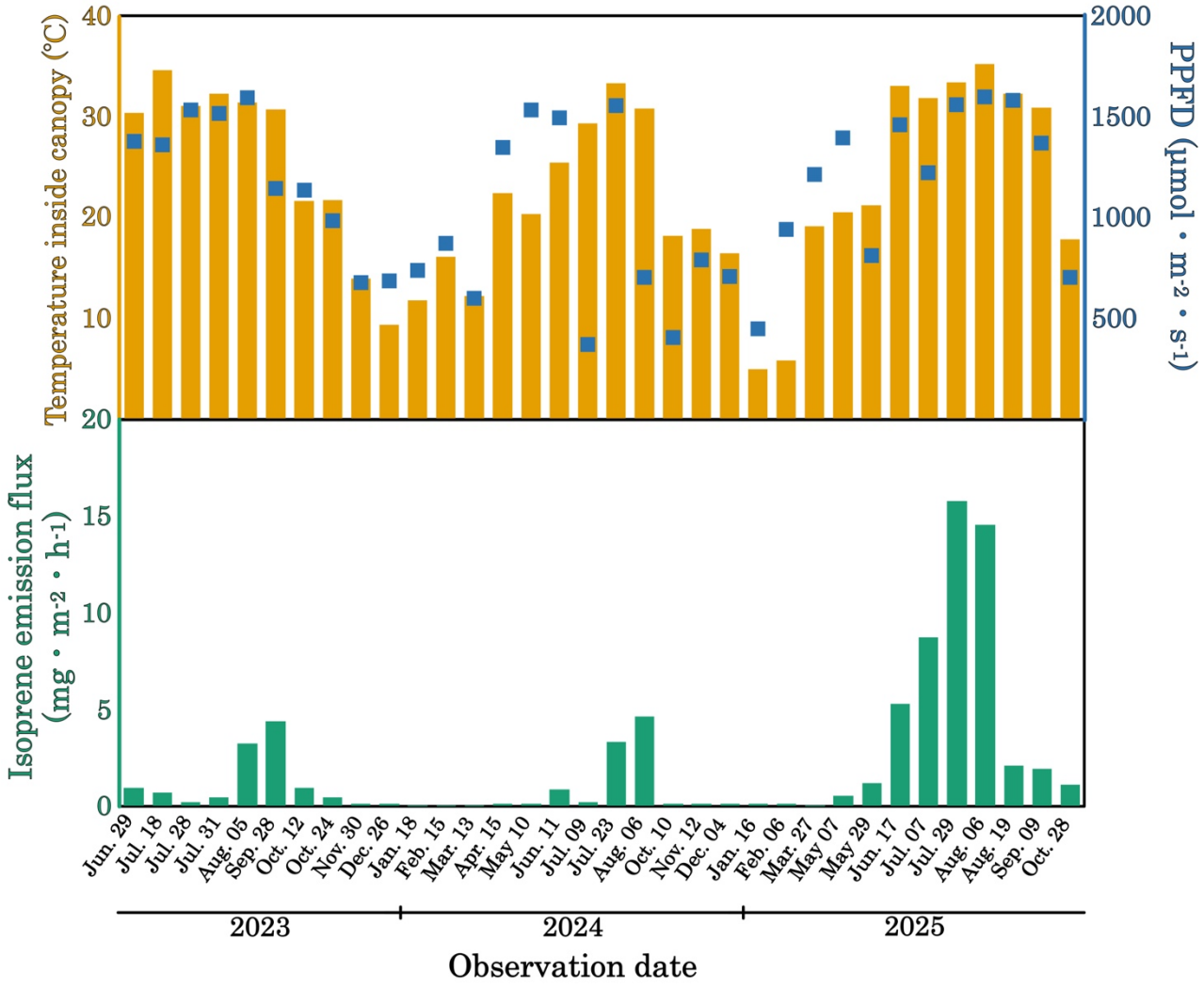

Figure 5: Daily average isoprene emission fluxes estimated from tower-based measurements (green bar graph), together with canopy temperature (orange bar graph) and PPFD (blue filled square) during the observation days from June 2023 to October 2025. Fluxes were calculated from the concentration gradient between 23 and 30 m using the aerodynamic gradient method.

420

Table 1. Daily average isoprene emission flux, friction velocity, diffusion coefficient, canopy temperature, PPFD, and LAI during the observation days.

Year	Month	Day	F_{obs} (mg m^{-2} h^{-1})			u^* (m s^{-1})			K (m^2 s^{-1})			Canopy Temp. (°C)			PPFD (μmol m^{-2} s^{-1})			LAI		
			Ave.	±	Std.	Ave.	±	Std.	Ave.	±	Std.	Ave.	±	Std.	Ave.	±	Std.	Ave.	±	Std.
2023	Jun.	29	0.95	±	0.70	0.46	±	0.05	0.48	±	0.19	30.4	±	1.3	1360	±	639	2.80	±	0.44
	Jul.	18	0.63	±	0.86	0.62	±	0.10	0.58	±	0.13	34.6	±	0.6	1340	±	447	2.67	±	0.52

	Jul.	28	0.21	±	0.85	0.85	±	0.21	0.66	±	0.03	31.1	±	1.0	1513	±	376	3.19	±	0.43
	Jul.	31	0.43	±	0.28	0.83	±	0.22	0.65	±	0.06	32.2	±	0.2	1497	±	403	3.19	±	0.43
	Aug.	5	3.21	±	2.55	1.03	±	0.28	0.74	±	0.09	31.4	±	0.9	1577	±	304	2.94	±	0.58
	Sep.	28	4.22	±	3.95	0.52	±	0.13	0.59	±	0.15	30.7	±	1.7	1127	±	398	2.77	±	0.63
	Oct.	12	0.92	±	0.68	0.47	±	0.17	0.61	±	0.17	21.6	±	0.7	1116	±	469	2.85	±	0.43
	Oct.	24	0.45	±	0.20	0.41	±	0.13	0.57	±	0.16	21.7	±	0.7	967	±	427	3.42	±	0.47
	Nov.	30	0.01	±	0.06	0.62	±	0.25	0.67	±	0.11	13.9	±	1.4	656	±	420	2.23	±	0.63
	Dec.	26	0.00	±	0.03	0.77	±	0.17	0.67	±	0.07	9.4	±	0.7	668	±	326	2.36	±	0.22
2024	Jan.	18	-0.05	±	0.05	0.44	±	0.10	0.66	±	0.14	11.8	±	1.3	717	±	269	1.98	±	0.58
	Feb.	15	-0.02	±	0.03	0.78	±	0.25	0.65	±	0.08	16.1	±	1.3	853	±	341	1.58	±	0.35
	Mar.	13	-0.04	±	0.06	1.40	±	0.15	1.10	±	0.09	12.2	±	0.7	579	±	374	1.02	±	0.21
	Apr.	15	0.08	±	0.06	0.81	±	0.29	0.73	±	0.06	22.5	±	0.9	1329	±	467	1.59	±	0.07
	May	10	0.08	±	0.06	0.81	±	0.29	0.73	±	0.06	20.4	±	0.1	1513	±	379	3.06	±	0.63
	Jun.	11	0.83	±	0.35	0.91	±	0.15	0.66	±	0.05	25.4	±	0.4	1474	±	462	2.25	±	0.46
	Jul.	9	0.25	±	0.40	0.25	±	0.07	0.10	±	0.05	29.3	±	0.5	350	±	243	2.91	±	0.62
	Jul.	23	3.26	±	2.60	0.58	±	0.09	0.51	±	0.07	33.3	±	0.8	1537	±	425	3.16	±	0.79
	Aug.	6	4.53	±	4.60	0.45	±	0.08	0.38	±	0.10	30.8	±	0.9	684	±	284	3.02	±	0.42
	Oct.	10	0.09	±	0.10	0.77	±	0.08	0.46	±	0.09	18.2	±	0.5	385	±	212	2.56	±	0.44
	Nov.	12	0.01	±	0.10	0.59	±	0.14	0.52	±	0.14	18.9	±	0.7	772	±	415	2.52	±	0.50
	Dec.	4	0.00	±	0.00	0.78	±	0.17	0.65	±	0.14	16.5	±	0.5	686	±	363	2.19	±	0.14
2025	Jan.	16	0.00	±	0.00	0.60	±	0.09	0.62	±	0.09	5.0	±	0.8	429	±	106	1.33	±	0.15
	Feb.	6	0.00	±	0.00	0.72	±	0.12	0.70	±	0.07	5.8	±	1.1	922	±	320	1.03	±	0.27
	Mar.	27	0.00	±	0.01	0.63	±	0.13	0.49	±	0.20	19.1	±	1.3	1195	±	422	1.50	±	0.22
	May	7	0.56	±	0.11	1.05	±	0.11	0.72	±	0.10	20.5	±	0.8	1376	±	555	3.02	±	0.82
	May	29	1.14	±	1.07	0.48	±	0.06	0.38	±	0.07	21.2	±	0.6	793	±	388	2.17	±	0.41
	Jun.	17	5.11	±	3.75	0.53	±	0.13	0.51	±	0.10	33.1	±	0.6	1443	±	510	2.83	±	0.75
	Jul.	7	8.43	±	10.85	0.42	±	0.19	0.46	±	0.15	31.9	±	0.4	1205	±	366	3.06	±	0.49
	Jul.	29	15.30	±	9.34	0.56	±	0.17	0.52	±	0.10	33.4	±	0.9	1538	±	417	2.88	±	0.37
	Aug.	6	14.02	±	15.33	0.53	±	0.18	0.54	±	0.04	35.3	±	0.3	1579	±	305	2.92	±	0.62
	Aug.	19	2.04	±	1.93	0.54	±	0.11	0.54	±	0.03	32.3	±	0.7	1563	±	180	2.92	±	0.62
	Sep.	9	1.90	±	3.02	0.49	±	0.16	0.49	±	0.08	30.9	±	0.7	1350	±	293	2.83	±	0.53
	Oct.	28	1.04	±	0.60	0.38	±	0.10	0.38	±	0.18	17.9	±	0.9	684	±	343	2.74	±	0.44

Positive isoprene fluxes were mainly observed during the warm-season sampling days, especially from June to September. Fluxes were generally low during the cold-season observations and during early spring. High fluxes were observed on several summer sampling days, particularly in 2025. As the sampling was intermittent and meteorological conditions

differed among observation days, these differences should be interpreted as variations among sampled summer conditions rather than indicating an interannual trend. Possible meteorological controls are discussed in Section 4.1.

Figure S6 shows the relationships between the isoprene flux and canopy temperature, PPFD, and LAI using the unaveraged dataset (n=263). As isoprene emissions exhibit exponential or saturated nonlinear responses to temperature, PPFD, and LAI (Guenther et al., 1993, 2006; Yu et al., 2017), Spearman's rank correlation coefficient (r_s) was used. Canopy temperature (r_s=0.71, $p < 0.001$), PPFD (r_s=0.49, $p < 0.001$), and LAI (r_s=0.58, $p < 0.001$) showed positive monotonic relationships with isoprene flux. These relationships are consistent with the known temperature, light, and phenological controls on isoprene emissions. However, because the dataset was obtained from intermittent daytime sampling, these correlations should be interpreted as relationships within the sampled conditions rather than as a comprehensive characterization of seasonal or interannual controls.

To further examine the combined effects of temperature and light, we also examined the relationship among F_{obs}, canopy temperature, and PPFD using a three-dimensional scatter plot (Fig. S7). Under high temperature and high PPFD conditions, F_{obs} tended to be high. However, some data points showed relatively low F_{obs} even when both canopy temperature and PPFD were high. This result indicates that temperature and light were important drivers of isoprene flux under the sampled daytime conditions, but they did not fully explain the observed flux variability. To analyze the factors involved, we first calculated the 75th percentile (Q3) for both temperature and PPFD from the entire observation dataset (n=263). We then extracted data points simultaneously satisfying temperature ≥ Q3 (approximately 32°C) and PPFD ≥ Q3 (approximately 1571 μmol m^{-2} s^{-1}). The F_{obs} distribution of this subset (n=37) was classified as follows. L-F_{obs} denotes the group below the 25th percentile (approximately 1.5 mg m^{-2} h^{-1}, n=10), and corresponds to the data points marked with black circles in Fig. S7. Although we were unable to identify a clear cause for the occurrence of L-F_{obs}, other factors, such as canopy-scale source distribution, local light environment, turbulent transport, concentration-gradient uncertainty, and tower-footprint representativeness, may also have contributed to the variability in F_{obs}.

3.4 Supplemental drone-based observations of horizontal variability

3.4.1 Horizontal variability in isoprene volume mixing ratios

Supplemental drone-based measurements were used to examine short-range horizontal variability in isoprene volume mixing ratios around the flux tower. Figure 6 shows the ratios of isoprene volume mixing ratios measured simultaneously at the tower and by the drone at a 30 m height. The average tower/drone ratios were 0.87 for the autumn observation at a horizontal distance of 15 m, 0.95 for the summer observation at 15 m, 1.32 for the summer observation at 30 m, and 0.99 for all data combined. These results indicate that isoprene volume mixing ratios around the tower differed by approximately 10% within 15 m and by up to approximately 30% at 30 m under the sampled conditions.

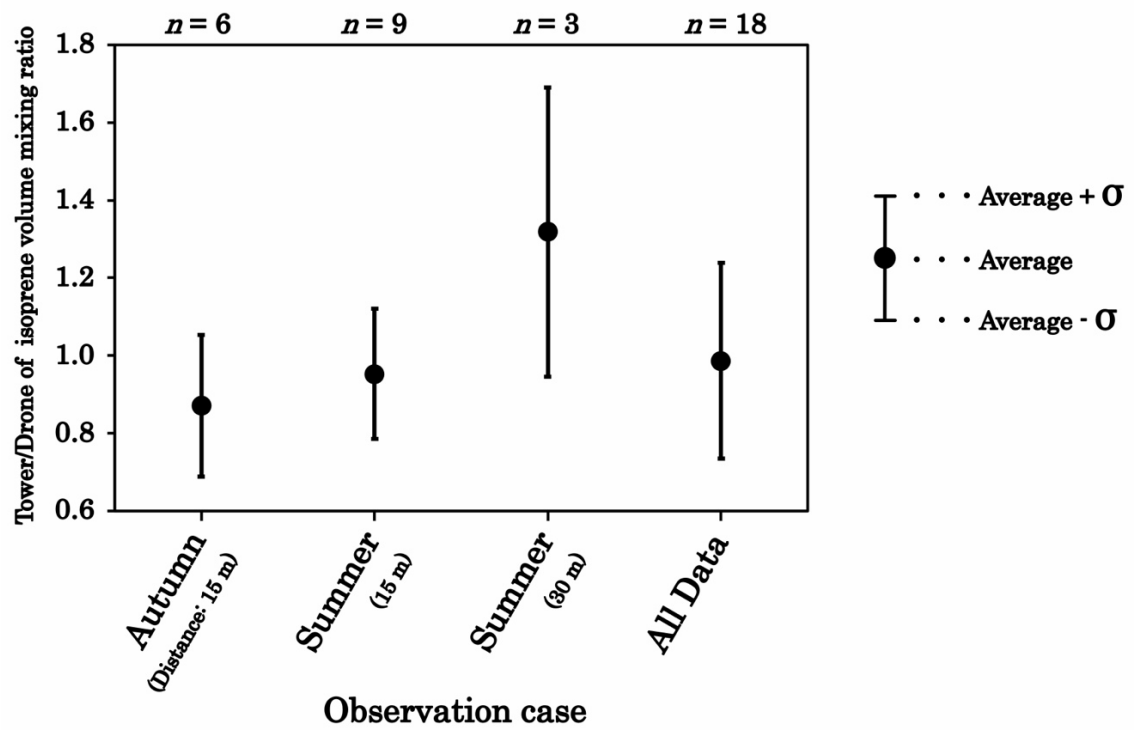

Figure 6: Ratios of isoprene volume mixing ratios measured simultaneously by the tower and drone at a 30 m height. Ratios are shown for the autumn observation at a 15 m horizontal distance, summer observations at 15 and 30 m horizontal distances, and all data combined. Points indicate average values, and error bars indicate ± standard deviation.

The scatter plot between the drone and tower measurements is shown in Fig. 7. The slope of the regression line was 1.05, and the Pearson correlation coefficient was $r = 0.96$ ($p < 0.001$), suggesting that the drone-based sampling captured variations broadly consistent with the tower measurements. However, because the drone observations were limited to selected days and short sampling periods, the results should be interpreted as an assessment of short-range horizontal variability rather than as a general characterization of spatial heterogeneity at the site. The larger differences observed at a 30 m distance may reflect small-scale heterogeneity in canopy structure, leaf density, light environment, and turbulent transport. These results suggest that even within several tens of meters of a flux tower, horizontal variability can contribute to uncertainty in the interpretation of fixed-point BVOC observations.

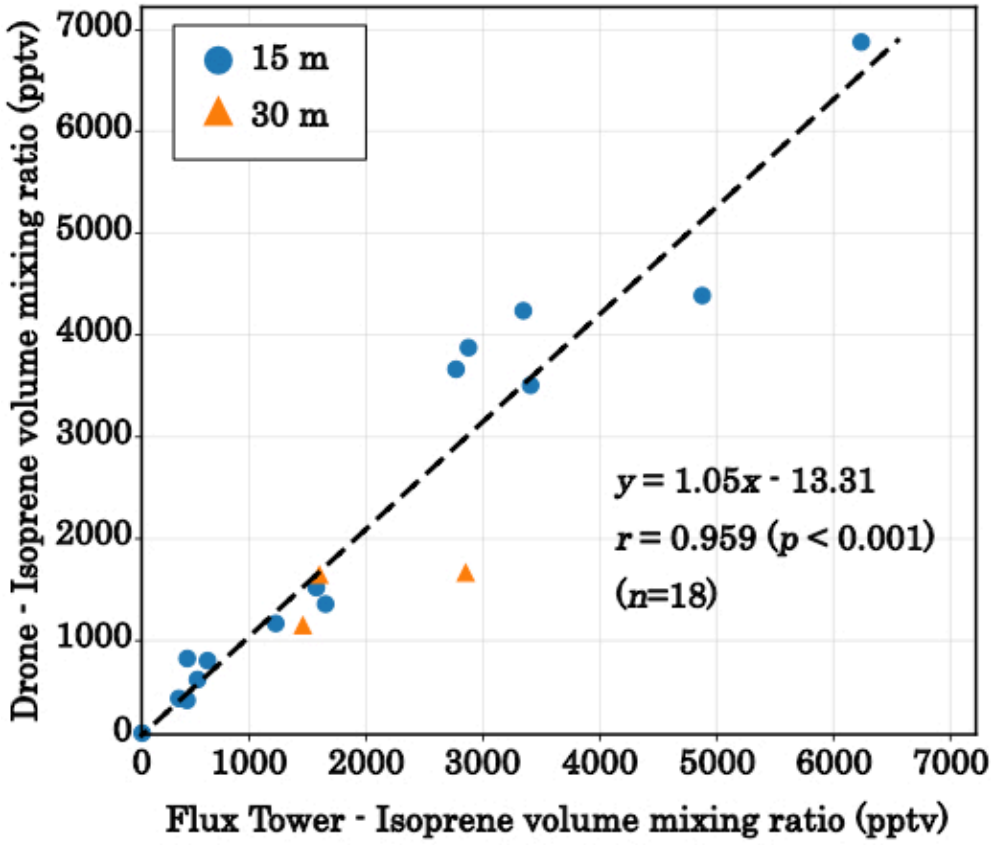

Figure 7: Comparison of isoprene volume mixing ratios measured simultaneously by the tower and drone at a 30 m height. The regression line and correlation coefficient are shown for all paired data.

3.4.2 Exploratory comparison of tower- and drone-derived flux estimates

Figure 8 shows the ratios of isoprene fluxes estimated from tower-based measurements at 23–30 m and drone-based measurements at 30–40 m. The average tower/drone flux ratios were 0.72, 0.98, and 0.85 for the 15 m, 30 m, and all-distance datasets, respectively. The all-distance dataset represents the combined 15 and 30 m drone sampling locations. Under conditions of a horizontal distance of 30 m, the flux ratios tended to approach 1 more than under conditions of 15 m. This indicates that the flux due to turbulent vertical transport is complex, and simply increasing the horizontal distance does not necessarily lead to different values.

The scatter plot of tower- and drone-derived isoprene fluxes is shown in Fig. 9. Although a positive correlation was observed between the two isoprene fluxes, it was not statistically significant when all data points were included ($y = 0.90x + 11.17$, $r = 0.44$, $p = 0.15$). However, when the two data points marked with black circles in the figure, which deviated significantly from the regression line, were excluded, the regression equation became $y = 0.67x + 7.74$, and $r = 0.74$ ($p = 0.015$), indicating a significant positive correlation between the two fluxes.

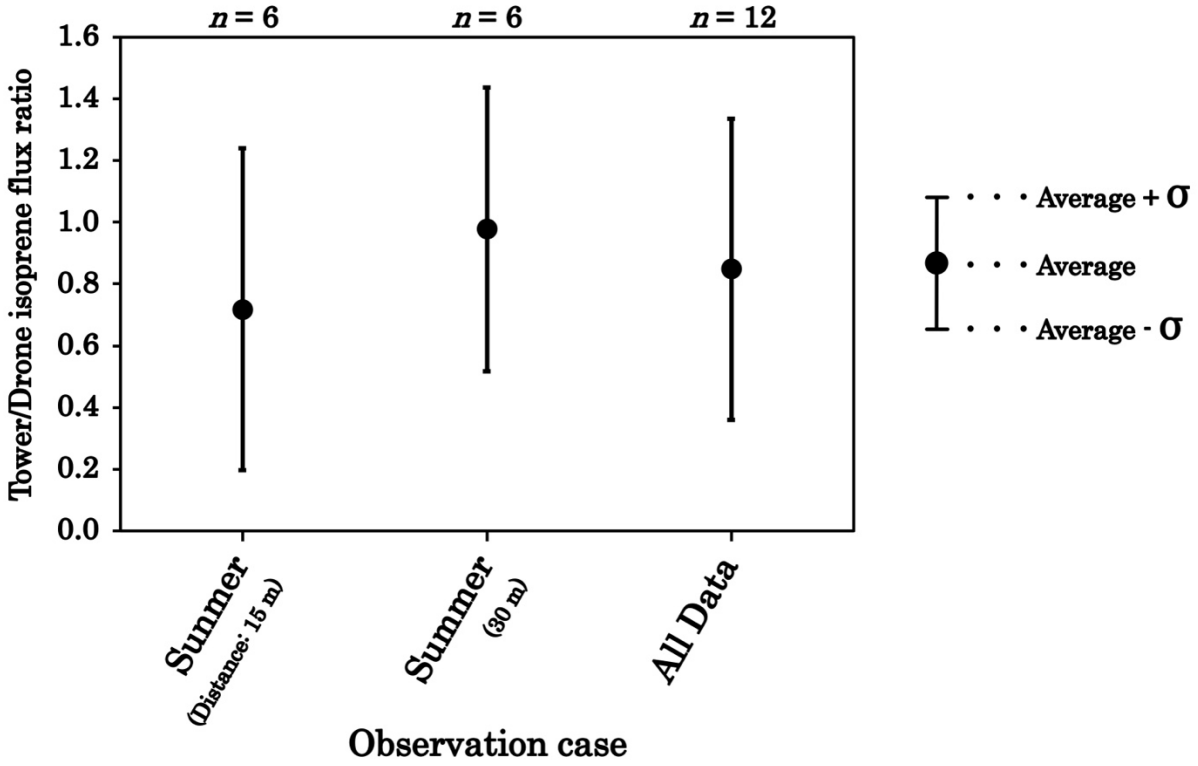

Figure 8: Ratios of tower-based and drone-based isoprene flux estimates during the supplemental drone experiment. Tower-based fluxes were calculated from the 23–30 m height interval, whereas drone-based fluxes were calculated from the 30–40 m height interval using tower-derived micrometeorological parameters. Points indicate average values, and error bars indicate ± standard deviation.

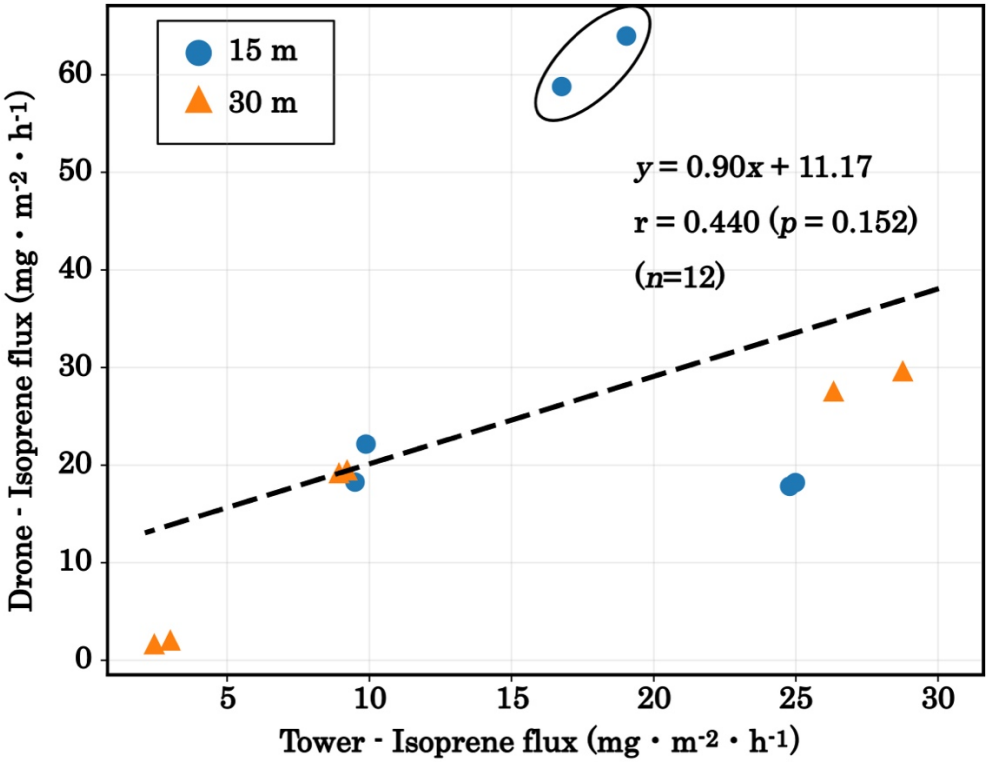

Figure 9: Exploratory comparison between tower-based and drone-based isoprene flux estimates. Tower-based fluxes were calculated from the 23–30 m height interval, whereas drone-based fluxes were calculated from the 30–40 m height interval using tower-derived micrometeorological parameters. The two data points that deviate from the regression line are marked with black circles.

The comparison should be interpreted cautiously because the tower- and drone-derived fluxes were calculated from different height intervals and the drone samples at 30 and 40 m were not collected simultaneously. In addition, micrometeorological parameters measured at the tower were used for the drone-based flux calculation because the drone could not carry a three-dimensional ultrasonic anemometer. Thus, the tower–drone flux comparison primarily reflects differences in concentration gradients, sampling height intervals, and sampling timing under tower-derived turbulence conditions, rather than directly measured differences in turbulent transport between the tower and drone locations. These methodological constraints likely contributed to the scatter in the tower–drone flux comparison. Accordingly, the drone-based flux analysis is treated here as an exploratory assessment of spatial representativeness and height-dependent uncertainty in gradient-based flux estimates. The results suggest that small-scale spatial variability and differences in sampling height can affect flux estimates, but additional observations are needed before this approach can be used for robust quantitative flux validation.

3.5 MEGAN comparison under the sampled conditions

3.5.1 Variations in calculated fluxes and activity factors

Figure S8 shows the daily average MEGAN-calculated isoprene fluxes (F_{cal}) from June 1, 2023 to October 31, 2025. Daily averages were calculated from the 10 min model outputs during the daytime sampling window from 10:00 to 16:00. Figure 10 shows the monthly variations in F_{cal} and the four activity factors γ_{LAI}, γ_P, γ_T, and γ_{age} from June 2023 to October 2025. Monthly statistics are summarized in Table S4.

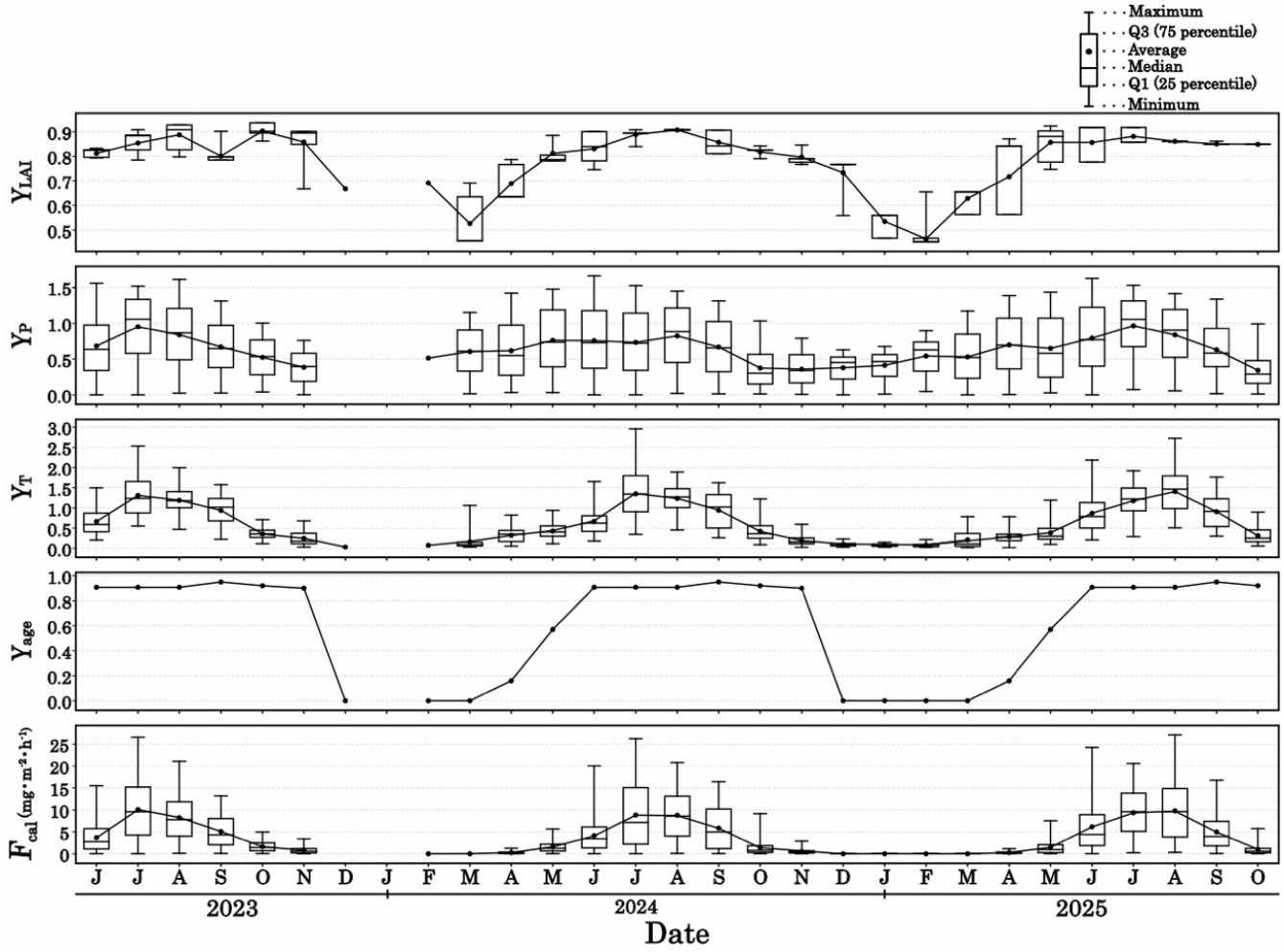

Figure 10: Monthly variation in the overlay of average values on the boxplots of MEGAN-calculated isoprene fluxes F_{cal} and the activity factors γ_{LAI}, γ_P, γ_T, and γ_{age}.

F_{cal} was generally low during the early spring leaf expansion period, increased during summer, and decreased toward the autumn leaf-fall period. This pattern reflects the combined effects of temperature, light, LAI, and leaf age in the MEGAN algorithm. Focusing on the summer months, which constitute the primary period for isoprene emission, the seasonal

averages (median values) were 7.4 (6.1), 7.3 (5.7), and 8.5 (7.6) mg m^{-2} h^{-1} for 2023, 2024, and 2025, respectively. Among the sampled summers, the calculated daytime fluxes tended to be higher in 2025.

γ_{LAI} began to rise gradually around early spring in March, and average values generally remained around 0.8–0.9 from May to October. γ_P maintained a base level of around 0.4–0.5 even during winter and increased to approximately 0.7–0.9 between June and August. γ_T showed large seasonal variation, with low values of around 0.1 during winter and average values of approximately 1.2–1.4 during July–August, suggesting it contributes significantly to the annual cycle F_{cal}. γ_{age} increased in spring, remained high from June through September, declined slightly from October to November, and dropped to 0 during the leaf-fall season.

To evaluate the relationship between F_{cal} and γ_P, γ_T, Spearman's rank correlation coefficients (r_s) were calculated using the 10 min data collected from May to October, when isoprene emissions were relatively high. The correlation coefficients were 0.86 for γ_P ($p < 0.001$) and 0.89 for γ_T ($p < 0.001$), indicating strong positive relationships. These relationships primarily reflect the structure of the MEGAN algorithm, in which light and temperature activity factors are major drivers of isoprene emission estimates under daytime conditions.

3.5.2 Comparison between observed and calculated fluxes

The comparison was performed using F_{obs} and F_{cal} for the period from April to October, when isoprene emissions were most evident, analyzing data from the observed days and time. The comparison included 24 observation days and 179 paired data points. As complete 10:00–16:00 observations were not available for all sampling days, the comparison was based only on available time-synchronized paired data. Gaps within the daytime sampling window may have increased the uncertainty of daily statistics because short-term variability within the day was not always fully captured. The data were summarized by season to examine whether model–observation differences varied among sampled phenological and meteorological conditions. As the number of paired data points differed among seasons, these seasonal statistics were used to describe model–observation differences within each sampled season rather than for evaluating complete seasonal model performance. The comparison is shown in Fig. 11, and Table 2 summarizes the MBE and RMSE.

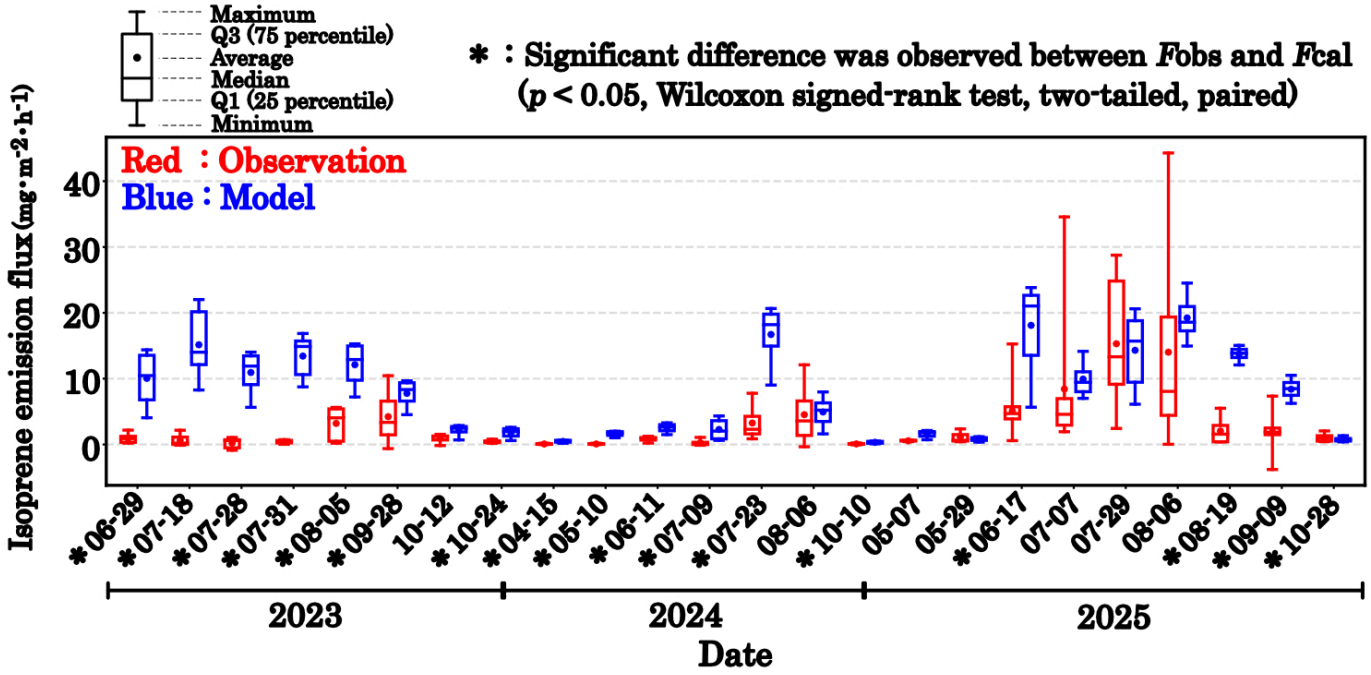

Figure 11: Comparison of observed tower-based isoprene fluxes (F_{obs}) and MEGAN-calculated fluxes (F_{cal}) for observation days from April to October.

Table 2. Number of data points (n) used for the comparison between F_{obs} and F_{cal} across spring, summer, and autumn data, along with calculated results for mean bias error (MBE) and root mean square error (RMSE).

	n	MBE[1)]	RMSE[1)]
April–May (Spring)	22	0.80	1.11
June–August (Summer)	112	7.20	10.54
September–October (Autumn)	45	2.16	3.76
Overall	179	5.15	8.56

1) unit: mg m^{-2} h^{-1}

For the entire April–October dataset, F_{cal} generally overestimated the F_{obs}, with MBE=+5.15 mg m^{-2} h^{-1} and RMSE=8.56 mg m^{-2} h^{-1}. The positive MBE indicates that MEGAN estimates were higher than observed fluxes on average under the sampled conditions. The relatively large RMSE indicates that the model–observation differences cannot be explained solely by a uniform offset and likely reflect variability in environmental responses, canopy representativeness, and observational flux uncertainty.

The discrepancy between MEGAN and observations was largest during the summer observation period. The MBE and RMSE were +0.80 mg m^{-2} h^{-1} and 1.11 mg m^{-2} h^{-1} for spring (n=22), +7.20 mg m^{-2} h^{-1} and 10.54 mg m^{-2} h^{-1} for summer

(n=112), and +2.16 mg m^{-2} h^{-1} and 3.76 mg m^{-2} h^{-1} for autumn (n=45), respectively. Spring showed smaller MBE and RMSE, whereas summer showed the largest positive bias and scatter. Autumn showed smaller errors than summer, although a positive bias remained. These seasonal differences suggest that model–observation discrepancies were larger under the sampled high-temperature and high-light conditions, when γ_T and γ_P were relatively large. Possible causes include uncertainties in basal emission rates, canopy microclimate, foliar temperature, canopy-scale representativeness, and AGM-based observed fluxes.

For each observation day, we evaluated the significance of daily distribution differences using the Wilcoxon signed-rank test (two-tailed, paired) with paired F_{obs} and F_{cal} data collected at the same time. The 22 d for which the number of daily pairs was at least five were included in the test. The remaining two days (May 7, 2025, and May 29, 2025) were excluded from the test because they had only three pairs. The test results showed significant differences ($p < 0.05$) on 17 of the 22 d. On 16 of those days, F_{cal} tended to be higher than F_{obs}.

Seasonal regression analysis using time-synchronized paired data and daily averages ($F_{cal} = a \times F_{obs} + b$) is shown in Fig. S9. For all seasons, the intercept was positive, suggesting that MEGAN tended to estimate non-negligible fluxes even when observed fluxes were low. The summer intercept was particularly large, indicating a tendency toward overestimation in the low F_{obs} range under the sampled summer conditions. Conversely, the slopes were below unity in summer and autumn, suggesting that the model did not fully reproduce the observed range of flux variability under the sampled conditions. These results highlight the need for further evaluation of MEGAN parameterizations using canopy-scale observations in suburban forest environments.

4. Discussion

4.1. Environmental controls on isoprene fluxes under sampled daytime conditions

The tower-based observations showed positive isoprene fluxes mainly during the warm-season sampling days, especially from June to September. The positive relationships between isoprene flux and canopy temperature, PPFD, and LAI indicate that the observed fluxes were influenced by temperature, light availability, and canopy development under the sampled daytime conditions. As the observations were conducted intermittently and did not cover complete diurnal cycles or all meteorological conditions, these relationships should be interpreted as tendencies within the sampled conditions rather than as a complete characterization of seasonal or interannual controls.

Isoprene production is strongly influenced by the availability of synthetic substrates, such as dimethylallyl diphosphate, generated through photosynthetic processes within chloroplasts, and by the activity of isoprene synthase. Photosynthesis depends on light availability, whereas isoprene synthase activity is strongly affected by temperature (Rasulov et al., 2010; Chen et al., 2022). Therefore, isoprene emissions are considered to correlate with temperature and PPFD. These physiological controls are consistent with the positive relationships observed between F_{obs}, canopy temperature, and PPFD in this study. However, according to Rasulov et al. (2010), the pool size of dimethylallyl diphosphate varies with temperature and decreases under high temperature conditions exceeding a threshold, suggesting that elevated temperatures may influence

isoprene emission rates. Guenther et al. (1993) observed the relationship between isoprene emission and leaf temperature in isoprene emitting trees—Sweetgum, Eucalyptus, Aspen, and Velvet bean. They reported that, depending on the tree species, the emission peak occurred at approximately 35°C, with emission levels decreasing above approximately 40°C. Exceeding the threshold temperature is thought to be associated with the inactivation of the synthetic substrate. In this study, the highest canopy air temperatures (maximum of 35.7°C) during sampling approached this range. However, leaf temperature was not measured directly, and canopy air temperature was used as a proxy. Therefore, the possible occurrence of thermal optimum or high-temperature suppression cannot be evaluated quantitatively from the present data.

Leaf phenology also likely contributed to the observed flux variability. Young leaves generally have lower isoprene emission capacity than mature leaves (Kuzma and Fall, 1993), and *Q. serrata* at FM Tama develops new leaves in spring and maintains mature leaves during summer. The low fluxes observed in early spring are therefore consistent with the expected lower emission capacity of young leaves, whereas higher fluxes during summer are consistent with mature foliage and favorable light and temperature conditions. LAI showed a positive relationship with isoprene flux, although this relationship is expected to saturate when canopy light availability becomes limiting (Yu et al., 2017).

Several high-flux events were observed during the summer 2025 sampling days. According to the Japan Meteorological Agency (2025), the 2025 rainy season ended earlier than usual, and in June and July, record-high temperatures were observed across northern, eastern, and western Japan, with the summer average temperature deviation reaching +2.36°C, significantly surpassing past records. This was attributed to the Tibetan anticyclone extending over Japan as a result of the upper-level westerlies flowing northward from June onward, influenced by the early and active development of the Asian monsoon. Furthermore, the expansion of the Pacific anticyclone coincided with this, bringing clear skies and rising temperatures. Consequently, the cumulative number of locations recording daily maximum temperatures of 40°C or higher also set a new record.

The average temperatures at FM Tama between 10:00 and 16:00 during the summers of 2023, 2024 and 2025 were 31.96°C, 29.34°C and 33.19°C respectively. Meanwhile, the average PPFD was not higher in 2025. Furthermore, no differences were observed in wind direction or wind speed among the observation days during the summer. This suggests that the high F_{obs} values in 2025 were likely associated with high-temperature sampling conditions. However, because the number of sampling days was limited and meteorological conditions differed among observation days, the present dataset cannot separate interannual variability from day-to-day meteorological variability.

Previous studies have shown that warming and heat-wave conditions can enhance BVOC emissions and influence atmospheric chemistry. Kramshøj et al. (2016) reported enhanced BVOC emissions under experimental warming in a tundra ecosystem, although the climate and vegetation differ substantially from those at FM Tama. Megaritis et al. (2013) predicted that a 2.5°C rise in temperature in Northern Europe would lead to an increase in BVOC emissions, resulting in a 20% increase in summer biogenic SOA. Moreover Churkina et al. (2017) estimated that increased BVOC emissions during heatwave events in the Berlin-Brandenburg metropolitan area of Germany contributed up to 60% of O_3 formation, indicating that the impact of BVOC increases due to high temperatures on the atmospheric environment is significant. Furthermore,

Wang et al. (2024) warn that during heat waves, plants not only increase the production of O_3 precursors but also close their stomata, thereby reducing O_3 removal by dry deposition; consequently, the increasing frequency of heat waves poses a major challenge for air pollution control. Therefore, continued BVOC flux observations under high-temperature conditions are important. Nevertheless, the present study should be regarded as providing observational evidence of high isoprene fluxes under selected hot daytime conditions, rather than a quantitative assessment of climate-change-driven trends in BVOC emissions.

4.2. Spatial representativeness and uncertainty of supplemental drone observations

The supplemental drone-based measurements provided information on short-range horizontal variability around the flux tower. The tower–drone comparison at a 30 m height indicated that isoprene volume mixing ratios differed by approximately 10% within 15 m and by up to approximately 30% at 30 m under the sampled conditions. These results suggest that even near a fixed flux tower, horizontal variability in canopy structure, leaf density, light environment, and turbulent transport can affect the interpretation of fixed-point BVOC observations.

However, the drone-based flux comparison should be interpreted with greater caution than the volume mixing ratio comparison. Drone-derived fluxes were calculated from the 30–40 m height interval, whereas tower-based fluxes were calculated from the 23–30 m height interval. In addition, the drone samples at 30 and 40 m were collected sequentially rather than simultaneously, and micrometeorological parameters measured at the tower were used because the drone could not carry a three-dimensional ultrasonic anemometer. Therefore, differences between tower- and drone-derived fluxes reflect not only horizontal variability in isoprene volume mixing ratios but also differences in the height interval, sampling timing, and assumed turbulence conditions.

Future drone-based BVOC flux studies would benefit from simultaneous multi-height sampling and direct turbulence measurements on or near the drone platform. As drone payload capacity and flight endurance improve through advances in battery technology, longer sampling periods and the installation of additional micrometeorological sensors may become possible. These developments would help reduce uncertainties in drone-based BVOC flux estimates and strengthen their role as a complementary approach to tower-based observations.

4.3 Possible causes of model–observation discrepancies in the MEGAN comparison

MEGAN generally overestimated the observed tower-based isoprene fluxes during the April–October sampling periods, with the largest MBE and RMSE during summer. As the comparison was based on time-synchronized paired data from intermittent daytime sampling, the results should be interpreted as model–observation differences under the sampled conditions rather than as a complete seasonal model evaluation. The larger summer discrepancy suggests that model uncertainties became more apparent under high-temperature and high-light conditions, when γ_T and γ_P were relatively large.

The larger summer discrepancy is important because summer is the period when isoprene emissions and photochemical activity are both enhanced. In urban and suburban environments, uncertainty in BVOC emission estimates can influence

simulations of O_3 and SOA formation, where biogenic precursors interact with anthropogenic nitrogen oxides. Therefore, reducing model–observation discrepancies under summer high-temperature and high-light conditions is important for improving BVOC emission estimates and their application to air quality modeling.

Both the observed fluxes and the MEGAN estimates include substantial uncertainties. The observed fluxes were estimated using the AGM, which depends on the measured concentration gradient, eddy diffusivity, stability correction, displacement height, and the assumption that the selected measurement heights were within a layer of approximately constant flux (Erisman and Draaijers 1995). In forest canopies, especially within or near the roughness sublayer, this assumption can be difficult to fully satisfy. Chemical loss or transformation of reactive BVOCs within and above the canopy may also influence the relationship between their emission and measured flux. Therefore, part of the model–observation discrepancy may reflect uncertainty in the observed flux estimates themselves.

Uncertainty in the basal emission rate (ε) is another likely source of discrepancy. MEGAN uses PFT-based standard emission factors, but these values may not fully represent the dominant species and local canopy conditions at FM Tama. Langford et al. (2017) raised concerns that ε in MEGAN was calculated based on a very limited number of leaf-level observations, resulting in considerable uncertainty. Tani et al. (2024) also emphasized that differences in measurement methods can cause variability in reported ε even for the same species. For *Q. serrata*, Okumura et al. (2008) reported leaf-level basal emission rates of 42.9 nmol m^{-2} s^{-1} for sunlit leaves and 20.5 nmol m^{-2} s^{-1} for shaded leaves. These values indicate that the emission capacity of *Q. serrata* can differ substantially between different leaf light environments. In the present study, we used the PFT-based standard emission factor in MEGAN to provide a baseline comparison with the tower-based flux observations. A full sensitivity analysis and validation using species-specific and sun/shade-specific emission factors would require additional assumptions regarding canopy structure, leaf area distribution, sunlit and shaded leaf fractions, and scaling from leaf-level emission capacity to canopy-scale fluxes. Such an analysis is therefore beyond the scope of the present study, but it represents an important next step for improving the MEGAN evaluation at this site.

The temperature response factor γ_T may also contribute to the discrepancy. In the present study, F_{cal} showed strong relationships with γ_T and γ_P, reflecting the structure of the MEGAN algorithm. Previous studies suggest that temperature response parameterizations may vary among ecosystems and species. Emmerson et al. (2020) measured isoprene using the leaf cuvette method across four Eucalyptus species at temperatures ranging from 293–328 K in 5 K increments, reporting that the temperature-dependent peak occurred at higher temperatures than those reported in the original MEGAN study. DiMaria et al. (2023) argued that ecosystem-specific γ_T parameterizations are needed to improve the representation of temperature sensitivity. At FM Tama, the high-temperature summer sampling conditions may have amplified uncertainties in the temperature response function and in the representativeness of canopy air temperature for leaf temperature.

Canopy-scale representativeness of the input variables is another important issue. MEGAN was driven by observed meteorological variables and LAI, but the actual foliar environment within the canopy can vary vertically and horizontally. Sunlit and shaded leaves experience different light and temperature conditions, and these differences may not be fully represented by tower-level PPFD, air temperature, or local LAI measurements. The drone observations also indicated short-

range horizontal variability in isoprene volume mixing ratios near the tower. These factors may partly explain why a uniform correction to MEGAN is insufficient to reproduce the observed flux variability.

Overall, the MEGAN comparison in this study should be interpreted as an evaluation under intermittent daytime sampling conditions. The results indicate potential sources of model–observation discrepancy, including basal emission factors, temperature response functions, canopy microclimate, spatial representativeness, and AGM-based flux uncertainty. However, because the observations were limited to selected daytime periods, the comparison does not represent a complete seasonal or annual model evaluation.

5. Summary and conclusion

This study conducted intermittent multi-year, multi-height BVOC observations at a 30 m flux tower in a suburban Tokyo forest dominated by *Quercus serrata* under a humid subtropical climate. Isoprene fluxes were estimated using the aerodynamic gradient method (AGM), and supplemental drone-based measurements were conducted on selected days to examine short-range horizontal variability around the tower. The observed tower-based fluxes were also compared with MEGAN estimates to evaluate model–observation agreement under the sampled daytime conditions. BVOC samples were collected at four heights, 30, 23, 17, and 3 m above ground level, during 34 sampling days from June 2023 to October 2025.

The tower observations showed that the volume mixing ratios of the target BVOCs were generally low during the cold-season sampling days (November–April), whereas those of isoprene increased markedly during warm-season sampling days (May–October). During peak summer observations, isoprene accounted for more than 90% of the measured BVOC composition. Isoprene volume mixing ratios were generally highest at 17 m, corresponding to the canopy layer, and higher values were also observed at 23 and 30 m above the main canopy during warm-season sampling. These vertical profiles indicate that enhanced isoprene volume mixing ratios were frequently observed within the *Q. serrata* canopy and that isoprene emitted from the canopy was transported upward. In contrast, monoterpene volume mixing ratios remained much lower than those of isoprene, and clear vertical gradients were not evident. These results indicate that isoprene was the dominant BVOC under the sampled warm-season daytime conditions at this site.

Tower-based isoprene fluxes estimated by AGM ranged from −0.05 to 15.30 mg m^{-2} h^{-1} on a daytime daily average basis. Positive fluxes were mainly observed during warm-season sampling days, especially from June to September. Several high-flux events were observed during summer 2025, when canopy temperatures during sampling were relatively high. However, because the observations were intermittent and meteorological conditions differed among sampling days, these differences should be interpreted as variations under sampled summer conditions rather than as evidence of an interannual trend. Isoprene fluxes showed positive relationships with canopy temperature, PPFD, and LAI, indicating that temperature, light availability, and canopy development were important controls on the observed fluxes under the sampled daytime conditions.

The supplemental drone-based measurements provided information on short-range horizontal variability around the tower. At a 30 m height, tower–drone comparisons showed that isoprene volume mixing ratios differed by approximately 10% within a horizontal distance of 15 m and by up to approximately 30% at 30 m under the sampled conditions. These results

suggest that even within several tens of meters of a flux tower, small-scale variability in canopy structure, light environment, and turbulent transport can influence the interpretation of fixed-point BVOC observations. Drone-derived flux estimates were also examined using the 30–40 m height interval, but these estimates should be regarded as exploratory because turbulence was not measured at the drone sampling points, the tower and drone used different height intervals, and the drone samples at 30 and 40 m were not collected simultaneously. Therefore, these drone measurements are interpreted as a supplementary approach for evaluating spatial representativeness and methodological uncertainty, rather than as an independent validation of tower-based fluxes.

The comparison between tower-based F_{obs} and MEGAN-calculated F_{cal} during April–October included 24 observation days and 179 time-synchronized paired data points. MEGAN generally overestimated the observed fluxes under the sampled conditions, with an overall MBE of +5.15 mg m^{-2} h^{-1} and RMSE of 8.56 mg m^{-2} h^{-1}. The discrepancy was largest during summer, when the MBE and RMSE were +7.20 and 10.54 mg m^{-2} h^{-1}, respectively. This larger summer discrepancy is important because isoprene emissions and photochemical activity are both enhanced under warm and high-light conditions, and uncertainties in BVOC emission estimates can influence simulations of O_3 and SOA formation in urban and suburban environments. Possible causes of the model–observation discrepancy include uncertainties in the basal emission rate, temperature and light response factors, canopy microclimate, foliar temperature, canopy-scale representativeness, and AGM-based observed fluxes.

As the observations were intermittent and limited to selected daytime periods, this study does not provide a complete diurnal, seasonal, or interannual characterization of BVOC emissions at FM Tama. Monthly, seasonal, and annual differences should therefore be interpreted as tendencies under sampled daytime conditions rather than as complete climatological patterns or long-term trends. Despite these limitations, this study demonstrates the potential and limitations of combining multi-height tower observations, supplemental drone-based sampling, and MEGAN comparison to evaluate BVOC fluxes and their spatial representativeness in a suburban forest environment. Future work should include more continuous tower-based BVOC flux measurements, direct turbulence measurements during drone sampling, simultaneous multi-height drone sampling, and sensitivity tests using *Q. serrata* specific basal emission rates and canopy microclimate information. Such improvements would help reduce uncertainties across leaf, canopy, and landscape scales and improve the use of BVOC observations for emission model evaluation and air quality modeling.

Code and data availability

The BVOC data observed in this study and the computational data from the MEGAN model are available from Zenodo (https://doi.org/10.5281/zenodo.21582015) and upon request to the corresponding author (ichikawa.yujiro@pref.saitama.lg.jp).

Author contributions

YI: Conceptualization, Data curation, Formal analysis, Funding acquisition, Investigation, Methodology, Project administration, Software, Validation, Visualization, Writing – original draft. KY: Investigation, Writing – review and editing. SY: Conceptualization, Funding acquisition, Methodology, Writing – review and editing. KT: Resources, Writing – review and editing. AS: Supervision, Writing – review and editing. KM: Resources, Supervision, Writing – review and editing. TO: Conceptualization, Funding acquisition, Methodology, Supervision, Writing – review and editing.

Competing interests

The contact author has declared that none of the authors has any competing interests.

Disclaimer

Publisher's note: Copernicus Publications remains neutral with regard to jurisdictional claims made in the text, published maps, institutional affiliations, or any other geographical representation in this paper. The authors bear the ultimate responsibility for providing appropriate place names. Views expressed in the text are those of the authors and do not necessarily reflect the views of the publisher.

Acknowledgements

Drone flight was assisted by Mr. Yuji Yamamoto and Mr. Hiroto Watanabe of Green Blue Co., Ltd. We would like to express our gratitude to them.

Financial support

This work was supported by Japan Society for the Promotion of Science KAKENHI (grant number 23K11413).

References

Altamira-Colado, E., Cuevas-González, D., Reyna, M. A., García-Vázquez, J. P., Avitia, R. L., and Osornio-Vargas, A. R.: Drone-assisted particulate matter measurement in air monitoring: A patent review, Atmosphere, 15, 515, https://doi.org/10.3390/atmos15050515, 2024.

Atkinson, R., and Arey, J.: Atmospheric degradation of volatile organic compounds, Chem. Rev., 103, 4605–4638. https://doi.org/10.1021/cr0206420, 2003.

Bai, J., Guenther, A. B., Turnipseed, A., Duhl, T., Yu, S., and Wang B.: Seasonal variations in whole-ecosystem BVOC emissions from a subtropical bamboo plantation in China, Atmos. Environ., 124, 12–21, https://doi.org/10.1016/j.atmosenv.2015.11.008, 2016.

Bai, J., Wu, Z., Yang, C., and Guenther, A.: Seasonal variations in whole–ecosystem BVOC emissions and ozone fluxes from a tropical rubber tree plantation in China, Atmos. Environ., 351, 121182, https://doi.org/10.1016/j.atmosenv.2025.121182, 2025.

Baker, B., Bai, J. H., Johnson, C., Cai, Z. T., Li, Q. J., Wang, Y. F., Guenther, A., Greenberg, J., Klinger L., Geron, C., Rasmussen, R.: Wet and dry season ecosystem level fluxes of isoprene and monoterpenes from a southeast Asian secondary forest and rubber tree plantation, Atmos. Environ., 39, 381–390, https://doi.org/10.1016/j.atmosenv.2004.07.033, 2005.

Bouvier-Brown, N. C., Schade, G. W., Misson, L., Lee, A., Mckay, M., and Goldstein, A. H.: Contributions of biogenic volatile organic compounds to net ecosystem carbon flux in a ponderosa pine plantation, Atmos. Environ., 60, 527–533, https://doi.org/10.1016/j.atmosenv.2012.06.070, 2012.

Chatani, S., Matsunaga, S. N., and Nakatsuka, S.: Estimate of biogenic VOC emissions in Japan and their effects on photochemical formation of ambient ozone and secondary organic aerosol, Atmos. Environ., 120, 38–50, https://doi.org/10.1016/j.atmosenv.2015.08.086, 2015.

Chen, Y.-J., Huang, Y.-L., Chen, Y.-H., Chang, S.-T., and Yeh, T.-F.: Biogenic volatile organic compounds and protein expressions of *Chamaecyparis formosensis* and *Chamaecyparis obtusa* var. formosana leaves under different light intensities and temperatures, Plants, 11, 1535. https://doi.org/10.3390/plants11121535, 2022.

Churkina, G., Kuik, F., Bonn, B., Lauer, A., Grote, R., Tomiak, K., and Butler, T. M.: Effect of VOC emissions from vegetation on air quality in Berlin during a heatwave, Environ. Sci. Technol., 51, 6120–6130, https://doi.org/10.1021/acs.est.6b06514, 2017.

DiMaria, C. A., Jones, D. B. A., Worden, H., Bloom, A. A., Bowman, K., Stavrakou, T., Miyazaki, K., Worden, J., Guenther, A., Sarkar, C., Seco, R., Park, J-H., Tota, J., Alves, E. G., and Ferracci, V.: Optimizing the isoprene emission model MEGAN with satellite and ground-based observational constraints, J. Geophys. Res., 128, e2022JD037822, https://doi.org/10.1029/2022JD037822, 2023.

Dumont, C., Verreyken, B. W. D., Schoon, N., Bergmans, B., Heinesch, B., and Amelynck, C.: Multi-year observations of BVOCs and ozone: concentrations and fluxes measured above and below the canopy in a mixed temperate forest, Earth Syst. Sci. Data, 18, 617-654, https://doi.org/10.5194/essd-18-617-2026, 2026.

Emmerson, K. M., Galbally, I. E., Guenther, A. B., Paton-Walsh, C., Guerette, E.-A., Cope, M. E., Keywood, M. D., Lawson, S. J., Molloy, S. B., Dunne, E., Thatcher, M., Karl, T., and Maleknia, S. D.: Current estimates of biogenic emissions from eucalypts uncertain for southeast Australia, Atmos. Chem. Phys., 16, 6997–7011, https://doi.org/10.5194/acp-16-6997-2016, 2016.

Emmerson, K. M., Possell, M., Aspinwall, M. J., Pfautsch, S., and Tjoelker, M. G.: Temperature response measurements from eucalypts give insight into the impact of Australian isoprene emissions on air quality in 2050, Atmos. Chem. Phys., 20, 6193-6206, https://doi.org/10.5194/acp-20-6193-2020, 2020.

EPA: https://www.epa.gov/sites/default/files/2019-12/documents/to-15a_vocs.pdf, last access: 29 April 2026.

Erisman, J. W., and Draaijers, G. P. J.: Atmospheric deposition in relation to acidification and eutrophication, Studies in Environmental Research 63, Elsevier, The Netherlands, 55–71, 1995.

Fares, S., Schnitzhofer, R., Jiang, X., Guenther, A., Hansel, A., and Loreto, F.: Observations of diurnal to weekly variations of monoterpene-dominated fluxes of volatile organic compounds from mediterranean forests: implications for regional modeling, Environ. Sci. Technol., 47, 11073–11082, https://doi.org/10.1021/es4022156, 2013.

Fuentes J. D. and Wang, D.: On the seasonality of isoprene emissions from a mixed temperate forest, Ecol. Appl., 9, 1118–1131, https://doi.org/10.1890/1051-0761(1999)009[1118:OTSOIE]2.0.CO;2, 1999.

Fuentes, J. D., Wang, D., and Gu, L.: Seasonal variations in isoprene emissions from a boreal aspen forest, J. Appl. Meteorol. Climatol., 38, 855–869, https://doi.org/10.1175/1520-0450(1999)038<0855:SVIIEF>2.0.CO;2, 1999.

Guenther, A. B., Zimmerman, P. R., Harley, P. C., Monson, R. K., and Fall, R.: Isoprene and monoterpene emission rate variability: Model evaluations and sensitivity analyses, J. Geophys. Res., 98, 12609–12617, https://doi.org/10.1029/93JD00527Digital Object Identifier, 1993.

Guenther, A., Hewitt, C. N., Erickson, D., Fall, R., Geron, C., Graedel, T., Harley, P., Klinger, L., McKay, W. A., Pierce, T., Scholes, B., Steinbrecher, R., Tallamraju, R., Taylor, J., and Zimmerman, P.: A global model of natural volatile organic compound emissions, J. Geophys. Res., 100, 8873–8892, https://doi.org/10.1029/94JD02950, 1995.

Guenther, A., Baugh, B., Brasseur, G., Greenberg, J., Harley, P., Serca, D., Vierling, L.: Isoprene emission estimates and uncertainties for the central African EXPRESSO study domain, J. Geophys. Res., 104 (D23), 30625–30639. https://doi.org/10.1029/1999JD900391, 1999.

Guenther, A. B., Karl, T., Harley, P., Wiedinmyer, C., Palmer, P. I., and Geron, C.: Estimates of global terrestrial isoprene emissions using MEGAN (Model of Emissions of Gases and Aerosols from Nature), Atmos. Chem. Phys., 6, 3181–3210, https://doi.org/10.5194/acp-6-3181-2006, 2006.

Guenther, A. B., Jiang, X., Heald, C. L., Sakulyanontvittaya, T., Duhl, T., Emmons, L. K., Wang, X.: The Model of Emissions of Gases and Aerosols from Nature version 2.1 (MEGAN2.1): an extended and updated framework for modeling biogenic emissions, Geosci. Model Dev., 5, 1471–1492, https://doi.org/10.5194/gmd-5-1471-2012, 2012.

Hayashi, K.: Atmospheric deposition 4. atmosphere-land exchange of substances, J. Jpn. Soc. Atmos. Environ. 45, A21-A31, 2010.

Holzinger, R., Lee, A., McKay, M., and Goldstein A. H.: Seasonal variability of monoterpene emission factors for a ponderosa pine plantation in California, Atmos. Chem. Phys., 6, 1267-1274, https://doi.org/10.5194/acp-6-1267-2006, 2006.

Ieda, T., Kitamori, Y., Mochida, M., Hirata, R., Hirano, T., Inukai, K., Fujinuma, Y., and Kawamura, K.: Diurnal variations and vertical gradients of biogenic volatile and semi-volatile organic compounds at the Tomakomai larch forest station in Japan, Tellus. Ser. B, Chem. Phys. Meteorol., 58, 177–186, https://doi.org/10.1111/j.1600-0889.2006.00179.x, 2006.

Ichikawa, Y., Nojiri, K., and Sasaka, K.: Determination of BVOCs based on high time-resolved measurements in urban and forest areas in Japan, Asian j. atmospheric environ., 17, 10, https://doi.org/10.1007/s44273-023-00009-6, 2023.

IPCC: https://www.ipcc.ch/report/ar6/wg1/, last access: 29 April 2026.

Japan Meteorological Agency: https://www.jma.go.jp/jma/press/2509/05b/kentoukai20250905.html, last access: 29 April 2026.

Kramshøj, M., Vedel-Petersen, I., Schollert, M., Rinnan, Å., Nymand, J., Ro-Poulsen, H., & Rinnan, R.: Large increases in Arctic biogenic volatile emissions are a direct effect of warming, Nat. Geosci., 9, 349–352, https://doi.org/10.1038/NGEO2692, 2016.

Kuzma, J., and Fall, R.: Leaf isoprene emission rate is dependent on leaf development and the level of isoprene synthase, Plant Physiol., 101, 435–440, https://doi.org/10.1104/pp.101.2.435, 1993.

Langford, B., Cash, J., Acton, W. J. F., Valach, A. C., Hewitt, C. N., Fares, S., Goded, I., Gruening, C., House, E., Kalogridis, A.-C., Gros, V., Schafers, R., Thomas, R., Broadmeadow, M., and Nemitz, E.: Isoprene emission potentials from European oak forests derived from canopy flux measurements: an assessment of uncertainties and inter-algorithm variability, Biogeosciences, 14, 5571–5594, https://doi.org/10.5194/bg-14-5571-2017, 2017.

Matsuda, K., Fujimura, Y., Hayashi, K., Takahashi, A., and Nakaya, K.: Deposition velocity of PM2.5 sulfate in the summer above a deciduous forest in central Japan, Atmos. Environ., 44, 4582–4587, https://doi.org/10.1016/j.atmosenv.2010.08.015, 2010.

Matsuda, K., Watanabe, I., Mizukami, K., Ban, S., and Takahashi, A.: Dry deposition of $PM_{2.5}$ sulfate above a hilly forest using relaxed eddy accumulation, Atmos. Environ., 107, 255–261, https://doi.org/10.1016/j.atmosenv.2015.02.050, 2015.

McKinney K. A., Lee, B. H., Vasta, A., Pho, T. V., and Munger, J. W.: Emissions of isoprenoids and oxygenated biogenic volatile organic compounds from a New England mixed forest, Atmos. Chem. Phys., 11, 4807–4831, https://doi.org/10.5194/acp-11-4807-2011, 2011.

McKinney, K. A., Wang, D., Ye, J., de Fouchier, J.-B., Guimarães, P. C., Batista, C. E., Souza, R. A. F., Alves, E. G., Gu, D., Guenther, A. B., and Martin, S. T.: A sampler for atmospheric volatile organic compounds by copter unmanned aerial vehicles, Atmos. Meas. Tech., 12, 3123-3135, https://doi.org/10.5194/amt-12-3123-2019, 2019.

Megaritis, A. G., Fountoukis, C., Charalampidis, P. E., Pilinis, C., and Pandis, S. N.: Response of fine particulate matter concentrations to changes of emissions and temperature in Europe, Atmos. Chem. Phys., 13, 3423–3443, https://doi.org/10.5194/acp-13-3423-2013, 2013.

Miyama, T., Okumura, M., Kominami, Y., Yoshimura, K., Ataka, M. and Tani A.: Nocturnal isoprene emission from mature trees and diurnal acceleration of isoprene oxidation rates near *Quercus serrata* Thunb. Leaves, J. For. Res., 18, 93–97, https://doi.org/10.1007/s10310-012-0350-5, 2013.

Mochizuki, T., Tani, A., Takahashi, Y., Saigusa, N., and Ueyama, M.: Long-term measurement of terpenoid flux above a *Larix kaempferi* forest using a relaxed eddy accumulation method, Atmos. Environ., 83, 53–61, https://doi.org/10.1016/j.atmosenv.2013.10.054, 2014.

Mochizuki, T., Miyazaki, Y., Ono, K., Wada, R., Takahashi, Y., Saigusa, N., Kawamura, K., and Tani, A.: Emissions of biogenic volatile organic compounds and subsequent formation of secondary organic aerosols in a Larix kaempferi forest, Atmos. Chem. Phys., 15, 12029–12041, https://doi.org/10.5194/acp-15-12029-2015, 2015.

Mochizuki, T., Takanashi, S., Wada, R., Miyazaki, Y., Nakano, T., & Tani, A.: Canopy fluxes of monoterpene, isoprene and isoprene oxidation products in a pine-oak forest. J. Agric. Meteorol., 76, 36–43. https://doi.org/10.2480/agrmet.D-19-00039, 2020.

Muñoz-Sabater, J., Dutra, E., Agustí-Panareda, A., Albergel, C., Arduini, G., Balsamo, G., Boussetta, S., Choulga, M., Harrigan, S., Hersbach, H., Martens, B., Miralles, D. G., Piles, M., Rodríguez-Fernández, N. J., Zsoter, E., Buontempo, C., and Thépaut, J.-N.: ERA5-Land: a state-of-the-art global reanalysis dataset for land applications, Earth Syst. Sci. Data, 13, 4349–4383, https://doi.org/10.5194/essd-13-4349-2021, 2021.

Naemura, A., Yoshikawa, T., Satoh, K., and Dokiya, Y.: Measurements of throughfall and stem-flow of *Cryptomermeria japonica* in Oku-chichibu and Tama Hills. Jpn. J. Biometeror., 39, 121–125, https://doi.org/10.11227/seikisho.39.121, 2003.

Okumura M, Tohno S, Tani A, Kominami Y, Miyama T, Takanashi S, and Kosugi Y: Isoprene emission characteristics of Quercus serrata in a deciduous broad-leaved forest. J. Agric. Meteorol., 64, 49–60, https://doi.org/10.2480/agrmet.64.49, 2008.

Penuelas, J., and Llusià, J.: Plant VOCs emissions: making use of the unavoidable, Trends Ecol. Evol., 19, 402–404, https://doi.org/10.1016/j.tree.2004.06.002, 2004.

Räisänen, T., Ryyppö, A., and Kellomäki, S.: Monoterpene emission of a boreal Scots pine (Pinus sylvestris L.) forest, Agric. For. Meteorol., 149, 808–819, https://doi.org/10.1016/j.agrformet.2008.11.001, 2009.

Rantala, P., Järvi, L., Taipale, R., Laurila, T. K., Patokoski, J., Kajos, M. K., Kurppa, M., Haapanala, S., Siivola, E., Petäjä, T., Ruuskanen, T. M., and Rinne, J.: Anthropogenic and biogenic influence on VOC fluxes at an urban background site in Helsinki, Finland, Atmos. Chem. Phys., 16, 7981–8007, https://doi.org/10.5194/acp-16-7981-2016, 2016.

Rasulov, B., Hüve, K., Bichele, I., Laisk, A., and Niinemets, Ü.: Temperature response of isoprene emission in vivo reflects a combined effect of substrate limitations and isoprene synthase activity: a kinetic analysis. Plant Physiol., 154, 1558–1570, https://doi.org/10.1104/pp.110.162081, 2010.

Seco, R., Karl, T., Turnipseed, A., Greenberg, J., Guenther, A., Llusia, J., Peñuelas, J., Dicken, U., Rotenberg, E., Kim, S., and Yakir, D.: Springtime ecosystem-scale monoterpene fluxes from Mediterranean pine forests across a precipitation gradient, Agric. For. Meteorol., 237, 150–159. https://doi.org/10.1016/j.agrformet.2017.02.001, 2017.

Sharkey, T. D., Wiberley, A. E., and Donohue, A. R.: Isoprene emission from plants: why and how, Ann. Bot., 101, 5–18, https://doi.org/10.1093/aob/mcm240, 2008.

Situ, S., Guenther, A., Wang, X., Jiang, X., Turnipseed, A., Wu, Z., Bai, J., and Wang, X.: Impacts of seasonal and regional variability in biogenic VOC emissions on surface ozone in the Pearl River delta region, China, Atmos. Chem. Phys., 13, 11803–11817, https://doi.org/10.5194/acp-13-11803-2013, 2013.

Tani, A., and Kawawata, Y.: Isoprene emission from the major native Quercus spp. in Japan, Atmos. Environ., 42, 4540–4550, https://doi.org/10.1016/j.atmosenv.2008.01.059, 2008.

Tani, A., and Mochizuki, T.: Review: Exchanges of volatile organic compounds between terrestrial ecosystems and the atmosphere, J. Agric. Meteorol., 77, 66–80, https://doi.org/10.2480/agrmet.D-20-00025, 2021.

Tani, A., Masui, N., Chang, T. W., Okumura, M., and Kokubu, Y.: Basal emission rates of isoprene and monoterpenes from major tree species in Japan: interspecies and intraspecies variabilities, Prog. Earth Planet. Sci., 11, 42, https://doi.org/10.1186/s40645-024-00645-8, 2024.

Wang, H., Nagalingam, S., Welch, A. M., Leong, C., Czimczik, C. I., and Guenther, A. B.: Heat waves may trigger unexpected surge in aerosol and ozone precursor emissions from sedges in urban landscapes, PNAS, 121, e2412817121, https://doi.org/10.1073/pnas.2412817121, 2024.

Wei, D., Fuentes, J.D., Gerken, T., Chamecki, M., Trowbridge, A. M., Stoy, P.C., Katul, G.G., Fisch, G., Acevedo, O., Manzi, A., von Randow, C, and dos Santos, R. M. N.: Environmental and biological controls on seasonal patterns of isoprene above a rain forest in central Amazonia, Agric. For. Meteorol., 256-257, 391–406, https://doi.org/10.1016/j.agrformet.2018.03.024, 2018.

Xu, M., Kasahara, K., Sorimachi, A., and Matsuda, K.: Nitric acid dry deposition associated with equilibrium shift of ammonium nitrate above a forest by long-term measurement using relaxed eddy accumulation, Atmos. Environ., 256, 118454, https://doi.org/10.1016/j.atmosenv.2021.118454, 2021.

Yang, W., Cao, J., Wu, Y., Kong, F., and Li, L.: Review on plant terpenoid emissions worldwide and in China, Sci. Total Environ., 787, 147454, https://doi.org/10.1016/j.scitotenv.2021.147454, 2020.

Yu, H., Guenther, A., Gu, D., Warneke, C., Geron, C., Goldstein, A., Graus, M., Karl, T., Kaser, L., Misztal, P., and Yuan, B.: Airborne measurements of isoprene and monoterpene emissions from southeastern U.S. forests, Sci. Total Environ., 595, 1498–1511, https://doi.org/10.1016/j.scitotenv.2017.03.262, 2017.